Dynamics, distribution, and transformations of mercury species from pyrenean high-altitude lakes

Bastien Duval, Emmanuel Tessier, Leire Kortazar, Luis Angel Fernandez, Alberto de Diego, David Amouroux

Journal Pre-proof

Dynamics, distribution, and transformations of mercury species from pyrenean high-altitude lakes

Bastien Duval, Emmanuel Tessier, Leire Kortazar, Luis Angel Fernandez, Alberto de Diego, David Amouroux

PII: S0013-9351(22)01938-7

DOI: https://doi.org/10.1016/j.envres.2022.114611

Reference: YENRS 114611

To appear in: *Environmental Research*

Received Date: 4 July 2022

Revised Date: 3 October 2022

Accepted Date: 16 October 2022

Please cite this article as: Duval, B., Tessier, E., Kortazar, L., Fernandez, L.A., de Diego, A., Amouroux, D., Dynamics, distribution, and transformations of mercury species from pyrenean high-altitude lakes, *Environmental Research* (2022), doi: https://doi.org/10.1016/j.envres.2022.114611.

CRediT Author Statements

Bastien Duval, Alberto de Diego and David Amouroux devised the research.

Bastien Duval wrote the manuscript.

Bastien Duval and Emmanuel Tessier performed all mercury measurements.

Acquisition of the financial support for the project leading to this publication by David Amouroux and Alberto de Diego.

All co-authors helped in the data interpretation and manuscript writing.

Dynamics, distribution, and transformations of mercury species from Pyrenean high-altitude lakes

Bastien Duval[*,1,2], Emmanuel Tessier[1], Leire Kortazar[2], Luis Angel Fernandez[2], Alberto de Diego[2], David Amouroux[*1]

[1]*Universite de Pau et des Pays de l'Adour / E2S UPPA, CNRS, Institut des Sciences Analytiques et de Physico-chimie pour l'Environnement et les Materiaux, UMR5254, Helioparc, 64053 Pau, France*

[2]*Kimika Analitikoa Saila, Euskal Herriko Unibertsitatea UPV/EHU, Sarriena Auzoa z/g, 48940 Leioa (Basque Country)*

**Corresponding authors*

Bastien Duval E-mail: bastien.duval@univ-pau.fr

David Amouroux E-mail: david.amouroux @univ-pau.fr

Abstract

While mercury (Hg) is a major concern in all aquatic environments because of its methylation and biomagnification pathways, very few studies consider Hg cycling in remote alpine lakes which are sensitive ecosystems. Nineteen high-altitude pristine lakes from Western / Central Pyrenees were investigated on both northern (France) and southern (Spain) slopes (1620 to 2600 m asl.). Subsurface water samples were collected in June 2017/2018/2019 and October 2017/2018 for Hg speciation analysis of inorganic mercury (iHg(II)), monomethylmercury (MMHg), and dissolved gaseous mercury (DGM) to investigate spatial and seasonal variations. In June 2018/2019 and October 2018, more comprehensive studies were performed in four lakes by taking water column depth profiles. Besides, in-situ incubation experiments using isotopically enriched Hg species (^{199}iHg(II), ^{201}MMHg) were conducted to investigate Hg transformation mechanisms in the water column. While iHg(II) (0.08 to 1.10 ng L^{-1} in filtered samples; 0.11 to 1.19 ng L^{-1} in unfiltered samples) did not show significant seasonal variations in the subsurface water samples, MMHg (<0.03 to 0.035 ng L^{-1} in filtered samples; <0.03 to 0.062 ng L^{-1} in unfiltered samples) was significantly higher in October 2018, mainly because of in-situ methylation. DGM (0.02 to 0.68 ng L^{-1}) varies strongly and can exhibit higher levels in comparison with other pristine areas. Depth profiles and incubation experiments highlighted the importance of in-situ biotic methylation triggered by anoxic conditions in bottom waters. In-situ incubations confirm that significant methylation, demethylation and photoreduction extents are taking place in the water columns. Overall, drastic environmental changes occurring daily and seasonally in alpine lakes are providing conditions that can both promote Hg methylation (stratified anoxic waters) and MMHg photodemethylation (intense UV light). In addition, light induced photoreduction is a major pathway controlling significant gaseous Hg evasion. Global warming and potential eutrophication may thus have direct implications on Hg turnover and MMHg burden in those remote ecosystems.

Keywords:

Mercury; Biogeochemistry; Alpine lakes; Methylation; Demethylation; Photoreduction

1. Introduction

Natural sources of mercury (Hg) (volcanic activities and degassing, evasion from aquatic and terrestrial surfaces) and increasing anthropogenic sources (e.g. fossil fuel combustion and gold mining), combined to a high volatility, contribute to the global pool of Hg in the atmosphere and lead to long-range dispersion and deposition away from point sources [1–3]. Hg has also created a scenario of global health concerns due to its conversion into an organometallic compound of elevated neurotoxicity, namely monomethylmercury (MMHg).

Hg is a biogeochemically driven contaminant because its most harmful organometallic species (MMHg) is naturally produced in aquatic systems thanks to a complex interplay between microbial and chemical processes. MMHg is a contaminant that biomagnifies from one trophic level to another, leading to elevated concentration on top of food chains. The European Water Framework Directive (WFD-2000/60/EG) classifies Hg as one of the 30th most "precarious dangerous pollutants". Human exposure to MMHg is well defined, and mainly associated with fish consumption [4]. Yet, most risk assessment studies lack fundamental information on what exactly controls Hg levels in fish. Without detailed knowledge of the Hg biogeochemical cycle and, in particular, the fundamental processes controlling MMHg production [5–7], it is difficult to precisely estimate Hg's health impacts and socio-economical costs [8].

The net production of MMHg in aquatic ecosystems is closely related to physical conditions and ecological characteristics, such as temperature, pH, organic matter, redox conditions, ionic strength and either solar radiation or the occurrence of microorganisms, that are able to transform various Hg compounds. Consequently, all these environmental settings have a direct influence on the Hg compounds reactivity or bioavailability, and regulate the extent of methylation, demethylation and reduction pathways [9]. MMHg bioaccumulation in aquatic food chains is largely dependent on these biotic and abiotic pathways that control its production and degradation or the removal of Hg from the ecosystem (e.g., volatilization, sedimentation). In most surface aquatic systems, a large array of conditions can control these various pathways according to geological, hydroecological or climatic conditions. However, the methylation of inorganic Hg (iHg(II)) in aquatic ecosystems is more specifically due to anaerobic microorganisms such as sulphate-reducing or iron-reducing bacteria, among other groups [10,11].

Among the aquatic compartments, lowland lakes have been widely studied regarding Hg pollution, speciation and species transformations [12–15]. Several studies highlighted a link between organic matter and Hg in lake ecosystems [13,16], with evidence of the catchment influence on the Hg levels. Significant photo-reduction and -demethylation were observed in lakes [17,18], exceeding the external inputs of MMHg (rain, snow, runoff) and therefore suggesting MMHg sources from bottom sediments. Nevertheless, the biogeochemical processes that control the speciation and fate of Hg, and especially MMHg levels, remain poorly established [12]. Alpine lakes are better witnesses of Hg past and present contamination in comparison with lowland lakes. They are usually characterized by a low catchment-to-lake-surface-area ratio, as the catchment surface is commonly smaller than lowland lakes. Therefore, atmospheric deposition and catchment weathering are important processes influencing greatly the lake water geochemistry [19]. Thus, mountain lake catchments are viewed and used as excellent proxies of background diffuse contamination [3,20]. While alpine lakes, through sediment cores analysis, have been successfully used to reconstruct temporal trends in atmospheric Hg deposition [2,3,21], Hg behaviour in the aquatic compartment of those pristine areas has been barely investigated. For instance, *Guédron et al.* [22,23] and *Alanoca et al*. [24] have reported Hg cycling features in high-altitude Bolivian lakes. Despite anthropogenic influences in these urban and mining areas, Hg species cycling is highly dynamic and MMHg production was driven by eutrophication in these lakes, while intense UV light promoted significant demethylation and reduction pathways. Regarding pristine high-altitude lakes, Hg species distribution has been only investigated in one study on four lakes from the French Alps [25]. Thus, while Hg transformations in the aquatic compartment have been well described in lower altitude or more accessible aquatic systems [15,24,26–33], there is a lack of studies in more pristine areas such as alpine lakes, particularly sensitive to global changes and long range transport of pollutants [20,34].

In that sense, *Chételat et al.* [12] suggested that profound environmental changes may be impacting the cycling and bioaccumulation of Hg. The responsibility of Humans on the dispersion of aerosols and Hg is undeniable [35,36], yet it is important to take into account the intensification of natural processes occurring through Global Change in the biogeochemical cycle of Hg species. In particular, Climate Change also accelerates many processes having an impact on alpine lakes dynamics: droughts and losses of snow cover that enhance dust production and soil runoff,

potential decreases of cloud density and ice cover period in lakes, surface waters temperature increase and water column stratification [20]. All these processes will have a direct effect on the aquatic cycling of Hg through enhance microbial or photochemical transformations of Hg or drastic changes in the transport of Hg via inputs to lake waters or sediments and atmospheric exchanges.

To better understand the potential role of global change of the Hg cycling in high altitude lakes, we report here for the first time a complete inventory of Hg levels and speciation (iHg(II), MMHg, DGM) as well as in situ measurements of Hg compounds transformation rates in the water column of alpine lakes from the Central - Western Pyrenees. The main objectives of this study were i) to assess the Hg species levels and variability in the aquatic compartment of these ecosystems, and better understand how seasonal or geographical conditions and lake trophic status may control such variability ii) to evaluate the importance of abiotic and biotic pathways affecting the fate of Hg in mountain lakes, and further estimate how selected lakes can be considered as sources of methylmercury and either enhance Hg burial or reemission iii) to highlight potential effects of climatic and biogeochemical changes on these identified pathways and their consequence on the future Hg cycling in remote and alpine aquatic environments.

2. Material and methods

2.1. Site description

The 19 studied high-altitude lakes (elevation: 1640 – 2600 m asl) are located in three different valleys of the Central-Western Pyrenees (France/Spain): Cauterets (n=7), Panticosa (n=9) and Ayous (n=3) areas (**see Figure 1, Figure A1 and Table A1**). These small lakes show similar physical properties (lake size: 0.37 – 12.82 ha; catchment size: 15 – 3229 ha; maximum depth: 3 – 35 m) but differ from their catchment characteristics and geological background, i.e. mainly granite core (pDe-GR) versus sedimentary rocks (Devonian, De-SR; Permo-Triassic, PT-SR; Cretaceous Cr-SR) [37,38]. Bioclimatic conditions are also substantially different with a decrease in temperature (2 – 19 °C), an increase in precipitation and an increase in the duration of the snow cover (50 – 246 days per year; determined according to *Gascoin et al.* [39] using data from Theia Snow collection (https://www.theia-land.fr/product/neige/) and published elsewhere (*Duval, PhD Thesis* [40]) at higher altitude. It is worth noting that the winter 2017 – 2018 was colder and/or with

much higher wet deposition and snow accumulation than the winters 2016 – 2017 and 2018 – 2019.

The water geochemistry of these lakes has been described elsewhere (*Duval, PhD Thesis* [40]) and the raw data are gathered in **Table A2**. Basically, despite the increase of the primary productivity during the summer (increasing Total Organic Carbon (TOC) associated to decreasing nitrate (NO_3^-)) and the influence of agropastoralism on lakes, all the studied lakes are classified as oligotrophic. The results, in accordance with previous Pyrenean lakes studies [19,41–43], highlighted the importance of the geological background, the atmospheric inputs, and, although very limited, the Human impact on the aquatic geochemistry of these high-altitude lakes.

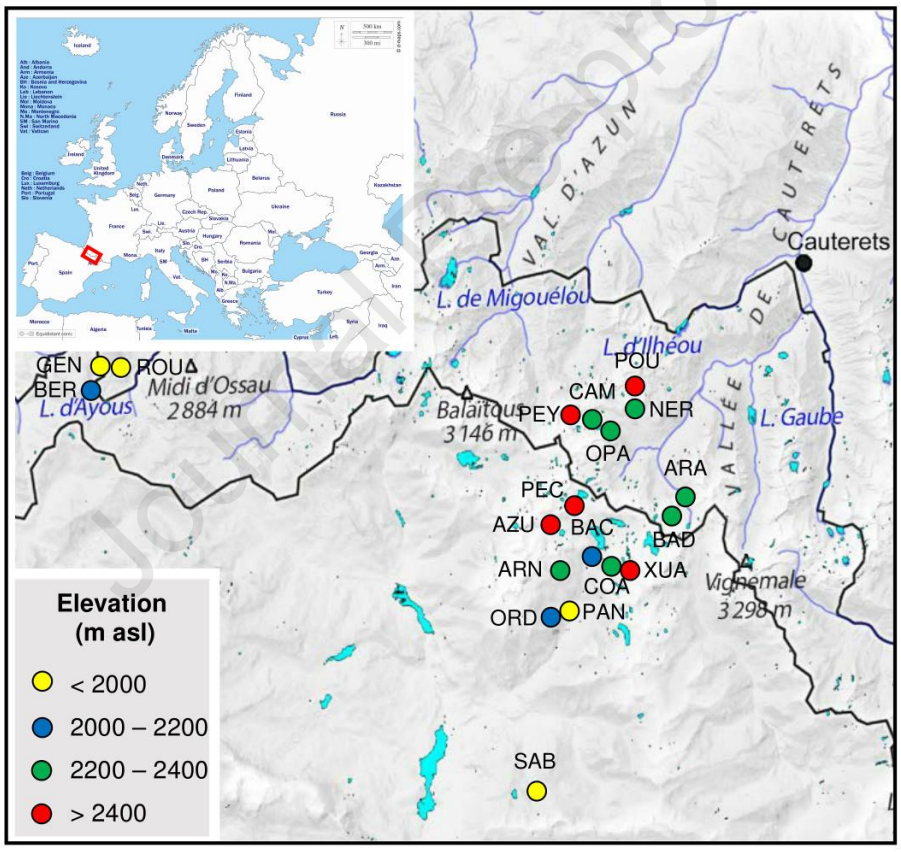

Figure 1 : Studied area; circles show position of the lakes, and colors indicate the elevation of the corresponding lakes. Lake acronyms are detailed in **Table A1**. See **Figure A1** for the whole map, including details about the geology of the lakes' catchment.

2.2. Water samples collection and processing

Subsurface (~0.5 m depth) water samples were collected during all the sampling campaigns (June 2017 [15 lakes, n=81]; October 2017 [10 lakes, n=58]; June 2018 [16 lakes, n=50]; October 2018 [16 lakes, n=40]; June 2019 [4 lakes, n=18]) with triplicate for the first two sampling campaigns to check for the spatial variability in the studied lakes. Additionally, water column profiles were investigated in Lac Gentau (GEN, 5 depths), Lac d'Arratille (ARA, 3 depths), Ibón de Sabocos (SAB, 6 depths) and Ibón Azul Alto (AZU, 3 depths), by sampling at different depths along the day. This study provides for the first time a unique Hg species data set with a total of 319 water samples (**Table A3 and Table A4**).

The particles in the water have a key role in the transport and fate of Hg species [16]. Thus, to evaluate their influence on the distribution of Hg species, two kinds of samples were collected and further analysed: filtered (F, dissolved fraction) and unfiltered (UF, total fraction). It is worth noting that considering the general oligotrophic status and elevation of the studied lakes, the particles were scarce and thus it was impossible to collect and analyse them.

Briefly, all the material needed up to the lake was transported by hiking. An inflatable rubber boat was used to reach the sampling locations. To collect the subsurface water samples, a manually operated ultra-clean sampler (*5L Teflon Coated Go-Flo Water Sampler, General Oceanic*) was deployed using powder-free gloves and avoiding the surface microlayer. For depth sampling, the Go-Flo sampler was deployed using a Kevlar cable and operated at the required depth with a plastic-coated messenger. Back ashore, the water sample was distributed with a clean silicone tubing in dedicated flasks according to the parameter to be further analysed.

First, an appropriate subsampling procedure was applied for dissolved gaseous Hg species (DGM). A 250 mL Teflon container was filled overflow without headspace and somehow following the protocol for the Winkler method (i.e. dissolved oxygen). Then, aliquots for unfiltered and filtered (Sterivex Filter unit, PVDF, 0.22 µm) non-gaseous Hg species (iHg(II), MMHg) were collected in 125 mL Teflon containers and acidified to 0.5 % v/v CH_3COOH 99% (Trace metal grade) [33]. The Teflon containers were closed tightly and stored in double PE Zip-lock bags in a portable cooler (5 – 10 °C), protected from light.

Other methods used for the measurement of ancillary parameters (conductivity, pH, temperature, dissolved oxygen saturation, chlorophyll-a, total organic carbon TOC, dissolved

inorganic carbon DIC, total alkalinity TA, silicate, sulphate SO_4^{2-}, chloride Cl^-, nitrate NO_3^-) are described elsewhere (*Duval, PhD Thesis* [40]).

2.3. Non-gaseous Hg species (iHg(II), MMHg) analysis

The quantification of non-gaseous Hg species (i.e. iHg(II) and MMHg) was carried out by double species-specific isotopic dilution method (D-SS-IDA) and analysis by capillary GC-ICP-MS [33,44]. Note that this analytical methodology allows to quantify the iHg(II) and the methylated species (MeHg, i.e., the sum of MMHg and DMHg,). Nevertheless, the purge sample experiment (**see Appendix 1 and Figure A2**) highlights the fact that the measured MeHg are mainly in the form of MMHg. LoD ranged from 9 to 34 pg L^{-1} for iHg(II) and from 3 to 4 pg L^{-1} for MMHg, in good agreement with recent publications [33,44].

Repeatability of the analytical measurement (n=3) was 2% for both iHg(II) and MMHg. The relative standard deviations (RSD) associated to the samples collected at three different locations of each lake (intra-lake variability, two first sampling campaigns) are 15 and 20% respectively for unfiltered and filtered MMHg, and 17 and 20% respectively for unfiltered and filtered iHg(II) and will be used to describe uncertainties in this paper.

2.4. Gaseous Hg species (DGM) analysis

The samples for gaseous Hg species (DGM) were processed close to the sampling site within 1 to 4 hours after sampling by stripping out and trapping the volatile Hg species from the water sample into a gold-coated sand trap [45,46]. For that purpose, the water sample was gently transferred into a Teflon purge vessel and subsequently purged under an argon flow (500 mL min^{-1}, 20 min). The moisture in the gas stream was eliminated by a cold trap (- 20 °C) before gaseous Hg collection in the gold-based trap. A second gold trap was always positioned after the sampling trap to prevent atmospheric contamination. Gold traps were sealed with polypropylene Teflon-lined caps and stored in double PE Zip-lock bags, in the dark (< 4°C) until analysis. All this procedure was carried out in an on-field laboratory installed in a mountain hut close to the sampling site.

The analysis of gaseous Hg species was done by double amalgamation on gold-AFS (DA/Au-AFS) [46]. Thermodesorption efficiency was controlled by carrying out two consecutive

analyses of the gold-coated sand trap. Gaseous Hg quantification was done by external calibration of the DA/Au-AFS device using a controlled Hg(0) source. Finally, the analysis of purge blanks allowed us estimating the efficiency of the sample treatment procedure. Considering the five sampling campaigns, the purge efficiency was assessed to reach (95±3) % (n=12). Note that this analytical methodology allows the measurement of the sum of Hg(0) and volatile dimethylmercury (DMHg). Nevertheless, regarding the very small levels of methylated species (MeHg), i.e. the sum of MMHg and DMHg, in comparison with DGM, we can assume that DGM is mainly elemental mercury Hg(0).

LoD were quiet constant over the sampling campaigns, ranging from 0.1 to 0.5 pg L^{-1}, which is consistent with the LoD of 0.4 pg L^{-1} reported by *Bouchet et al.* [46].

2.5. Hg species transformation assessments

In-situ water incubation experiments over 7h (usually from 9 a.m. to 4 p.m. UTC+2) using isotopically enriched Hg species (^{199}iHg(II), ^{201}MMHg) were conducted in the June 2018, October 2018 and June 2019 campaigns at lakes Gentau, Arratille, and Sabocos to investigate Hg species transformation mechanisms in the water column (methylation, demethylation, reduction) according to the procedure published elsewhere [47–49].

Unfiltered water samples were collected to perform the incubation experiments. Different conditions of incubation were tested depending on sampling depth (subsurface, middle depth, and bottom) or light exposure (Diurnal vs Dark) (**Table A5**).

After collecting a water sample using Go-Flo sampler, a first set of samples was prepared. Three 125 mL Teflon container (triplicate) per condition were directly filled with the water sample up to the top. Isotopically enriched spikes were added to each of the replicate to obtain concentrations in ^{199}iHg(II) and ^{201}MMHg of respectively 2 and 0.2 ng L^{-1}. It corresponds to about 10 times the natural concentrations observed in the studied ecosystems: high enough to overlap the natural concentrations and low enough to avoid any biotic stress. Using a simple mooring line at the sampling point, incubation bottles, either protected from the light or not, were placed at the corresponding depth. After 7 hours, the Teflon containers were collected, and the incubation processes were stopped by adding high-purity HCl (1 % v/v). Teflon containers were closed tightly and stored in double PE Zip-lock bags in a portable cooler (5-10 °C), protected from light, and

259 further transported and stored in the laboratory (5-10 °C). This first set of samples allows the
260 determination of methylation, demethylation and MMHg loss rates.

261 A second set of samples was prepared to determine Hg reduction rates. After collection
262 of water using the Go-Flo sampler, two 250 mL Teflon containers (duplicate) per condition were
263 filled overflow without headspace and somehow following the protocol for the Winkler method and
264 spiked with 2 and 0.2 ng L^{-1} isotopically enriched ^{199}iHg(II) and ^{201}MMHg, respectively, like in the
265 previous case. They were incubated together with the samples of the first set. The difference in
266 this case is that, at the end of the 7 hours, the elemental Hg (Hg(0)) was immediately recovered
267 in gold-coated sand traps by purging the water samples.

268 Quantification was carried out by isotope pattern deconvolution (IPD) isotope dilution
269 analysis (IDA) and analysis by capillary GC-ICP-MS for the water samples following the same
270 protocol used for the determination of organomercury species [32]. The particularity is that the
271 samples were spiked with other enriched isotope solution (^{198}iHg(II) and ^{202}MMHg).

272 The gaseous species trapped in the gold-coated sand traps were quantified by IPD and
273 analysed by thermal desorption cryogenic trapping (CT) followed by GC-ICP-MS. Recoveries and
274 mass balance of the added Hg spikes during the experiment were systematically established in
275 order to provide accurate transformation yield as previously described [18,32,48].

276 The Hg species incubation experiment allowed us to calculate methylation (M) (iHg(II)
277 into MMHg), demethylation (D) (MMHg into iHg(II)), MMHg loss (L) (MMHg into iHg(II) and Hg(0))
278 and reduction (R) (iHg(II) into Hg(0)) potentials (in % day^{-1}) (**Figure A3**) according to *Rodriguez-*
279 *Gonzales et al.* [48] with the following formula:

280 $$Methylation\ (M) = \frac{0^{199}MMHg_t - 0^{199}MMHg_{t0}}{0^{199}iHg(II)_{t0}} \times \frac{1440}{t} \times 100$$

281 $$Demethylation\ (D) = \frac{0^{201}iHg(II)_t - 0^{201}iHg(II)_{t0}}{0^{201}MMHg_{t0}} \times \frac{1440}{t} \times 100$$

282 $$MMHg\ Loss\ (L) = \frac{0^{201}MMHg_{t0} - 0^{201}MMHg_t}{0^{201}MMHg_{t0}} \times \frac{1440}{t} \times 100$$

283 $$Reduction\ (R) = \frac{0^{199}Hg(0)_t - 0^{199}Hg(0)_{t0}}{0^{199}iHg(II)_{t0}} \times \frac{1440}{t} \times 100$$

where t is the time of incubation (min), $^{XXX}iHg(II)_{t0}$, $^{XXX}MMHg_{t0}$ and $^{XXX}Hg(0)_{t0}$ are the concentrations measured at the beginning of the incubation experiment, $^{XXX}iHg(II)_t$, $^{XXX}MMHg_t$ and $^{XXX}Hg(0)_t$ are the concentrations measured at the end of the incubation experiment.

To predict the variations of MMHg concentrations in the lake, the potential net Hg methylation (ng L^{-1} day^{-1}) was calculated using the methylation and demethylation rates (% day^{-1}) according to the following formula:

$$Net\ Methylation = \frac{M}{100} \times [iHg(II)]_{ambient} - \frac{D}{100} \times [MMHg]_{ambient}$$

where M is the methylation potential (% day^{-1}), $[iHg(II)]_{ambient}$ is the ambient iHg(II) concentration (ng L^{-1}), D is the demethylation potential (% day^{-1}), $[MMHg]_{ambient}$ is the ambient MMHg concentration (ng L^{-1}).

It is worth noting that we chose to use demethylation rates instead of MMHg loss rates to avoid an underestimation of the net methylation since we have only determined MMHg production from iHg(II). Thus, in that case, we specifically consider the most significant reversible methylation/demethylation pathways between iHg(II) and MMHg forms.

2.6. Hg gaseous fluxes at the air-water interface

According to *Sharif et al.* [32], gaseous Hg fluxes at the air-water interface (volatilization flux densities [FD]) (ng m^{-2} h^{-1}) were calculated using the following equation:

$$\text{Volalitization FD} = k_W \times ([\text{DGM}] - \frac{[TGM]}{H})$$

where DGM is the concentration of DGM (i.e. $Hg(0)_{aq}$) measured in the subsurface water (ng m^{-3}), TGM is the concentration of TGM (i.e. $Hg(0)_g$) measured in the atmosphere. As a reference value for atmospheric concentration of TGM we used the measurement performed at the Pic du Midi (2860 m asl.) between February 2012 and January 2013 [50] (1.8 ng m^{-3}). H is the dimensionless Henry's Law constant corrected for water temperature and salinity [51] and k_W is the Hg(0) gas transfer velocity (m h^{-1}) at the air-water interface. k_W was calculated, according to *Sharif*

308 *et al.* [32] and using a specific model developed for CO_2 exchanges in sheltered lakes [52], as a
309 function of wind speed.

310 The wind speed has been measured during daytime in Lake Gentau (w = (3.2 ± 1.4) m s^{-1} in June
311 2018; w = (1.4 ± 0.8) m s^{-1} in October 2018; w = (2.6 ± 2.0) m s^{-1} in June 2019), Lake Sabocos
312 (w = (1.5 ± 1.2) m s^{-1} in June 2018; w = (2.8 ± 2.1) m s^{-1} in October 2018; w = (2.0 ± 2.0) m s^{-1} in
313 June 2019), Lake Arratille (w = (1.5 ± 0.7) m s^{-1} in June 2018) and Lake Azul (w = (0.8 ± 0.8) m
314 s^{-1} in June 2018). Thus, to estimate the FD in all the sampled lakes, two wind speed ranges will
315 be considered: smooth breeze at 1 m s^{-1} to stronger wind at 3 m s^{-1}, which corresponds well to
316 sheltered lakes conditions as proposed by *Cole and Caraco* [52].

317 # 3. Results and discussion

318 ## 3.1. Total Hg (Hg_{TOT}) in all lake waters

319 The concentrations of iHg(II) and MMHg, both in filtered (F) and unfiltered (UF) samples,
320 and DGM are presented in **Table A3** and their variability is illustrated in **Figure 2.** Total Hg (Hg_{TOT})
321 is defined here as the sum of concentrations of iHg(II), MMHg and DGM in unfiltered samples
322 (DGM only measured in unfiltered samples).

323 In the following discussions, to establish a proper global assessment of the total Hg
324 (Hg_{TOT}) in the subsurface water of the high-altitude lakes, seven outliers are discarded from the
325 whole database based on to the fact that the concentrations observed were too high compared
326 to the normal distribution of our data and that no valid explanation could be given for such higher
327 values (**see Appendix 2 for more details**). Hg_{TOT} is quite homogeneous along the five sampling
328 campaigns, ranging from 0.17 to 1.37 ng L^{-1} with a median value of 0.48 ng L^{-1} and an average
329 of (0.54 ± 0.26) ng L^{-1} (n=66). The homogeneity in the Hg_{TOT} concentrations in the Pyrenean lakes
330 suggests that local inputs through geogenic paths (erosion, lixiviation) are not significant and does
331 not play a key role in the biogeochemistry of Hg as it was found for other trace elements [38,43,53].
332 This also confirms the fact that Hg inputs in alpine environments like the Pyrenees are mainly due
333 to wet and dry atmospheric deposition. Only two previous studies showed that unfiltered Hg_{TOT}
334 varies from 2 to 14 ng L^{-1} in the precipitation from the Pyrenees (880 m asl) in 2014 [54] and from
335 2 to 170 ng L^{-1} in the surface snow from the Alps (2448 m asl) in 2008 – 2009 [55]. In our study, Hg

species in meltwater and ice were also measured in Lake Cambalès in June 2018. The Hg_{TOT} concentrations were much higher in ice (Hg_{TOT} = 19.41 ng L^{-1}) than in meltwater (Hg_{TOT} = 1.05 ng L^{-1}) and subsurface water (Hg_{TOT} = 0.45 ng L^{-1}). These reported concentrations in atmospheric depositions are much higher than the levels observed in the subsurface water from the high-altitude lakes from this study, suggesting a simple dilution effect or more complex exchanges in lake waters as discussed thereafter.

3.2. Mercury compounds distribution in water samples

3.2.1. Variability in subsurface waters of all lakes

Inorganic mercury (iHg(II)) (Figure 2)

Filtered and unfiltered iHg(II) levels ($iHg(II)_F$ and $iHg(II)_{UF}$) in subsurface water from the 19 sampled lakes over the five sampling campaigns were slightly lower than other worldwide lakes [15,22,24,25,28–31] and freshwaters from the same area [32,33] (**Table 1**). $iHg(II)_F$ ranges from 0.08 to 1.10 ng L^{-1} with a median value of 0.23 ng L^{-1} and $iHg(II)_{UF}$ ranges from 0.11 to 1.19 ng L^{-1} with a median value of 0.38 ng L^{-1}, similar to concentration levels found in marine waters [56,57] and typical from a pristine environment.

The filtered fraction of Hg ($iHg(II)_F$) represents about 68 ± 16 % (range from 19 to 100 %) of the unfiltered fraction ($iHg(II)_{UF}$), suggesting that most of the mercury in the Pyrenean lakes is found in the dissolved fraction. However, subsurface water samples from Azul in Spring 2017 (39 %), Peyregnets (47 %) and Gentau (19 % to 44 %) in Spring 2018 and Cambalès (41%), Peyregnets (49 %) and Gentau (41 %) in Autumn 2018 are exhibiting higher particulate Hg fraction.

On **Figure 2**, the homogeneity observed in the iHg(II) concentrations, either filtered or unfiltered, along the five different seasons demonstrates a rather steady state in the Hg mass balance between the investigated periods. Another study reports seasonal variations of iHg(II) in the high altitude subtropical Lake Uru Uru (3686 m asl) [24]. In that case, concentrations were significantly higher during the dry season over the wet season because of the enhanced evaporation occurring at the end of the dry season. In pristine Pyrenean lakes, the concentration

of iHg(II) in Autumn (2017 and 2018) is not significantly higher than in early Spring (2017, 2018 and 2019) (Kruskal-Wallis test, p-value = 0.79 and 0.54 respectively for $iHg(II)_{UF}$ and $iHg(II)_{F}$).

Monomethylmercury (MMHg) (Figure 2)

Filtered and unfiltered MMHg levels ($MMHg_F$ and $MMHg_{UF}$) in subsurface water from the 19 sampled lakes over the five sampling campaigns vary respectively from <0.003 to 0.035 ng L^{-1} and from <0.003 to 0.062 ng L^{-1} (**Table 1**). The median values, 0.008 for $MMHg_F$ and 0.011 for $MMHg_{UF}$, are typical from pristine aquatic environments, in the range of what has been found in Lake Superior ($MMHg_F$ = 0.005 ± 0.001 ng L^{-1} in April 2000; $MMHg_F$ = 0.008 ± 0.002 ng L^{-1} in August 2000) [15] and in some high-altitude lakes in the Alps (0.002 – 0.005 ng L^{-1}) [25]. MMHg represents (4±3) % of the filtered non-gaseous Hg and (4±2) % of the unfiltered non-gaseous Hg.

From Hg speciation analyses in surface snow from the French Alps (2448 m asl) *Marusczak et al.* [55] concluded that biotic production of MMHg in the snowpack is unlikely, considering the constant ratio MMHg/THg measured throughout the season in their study. The main contributor to Hg in the high-altitude lakes being atmospheric deposition, the higher proportion of MMHg observed in surface waters from high-altitude lakes in the Alps (4 ± 3 % for $MMHg_F$ and 3 ± 2 % for $MMHg_{UF}$) in comparison to surface snow (MMHg vary from non-determined to 1.21 % of the total Hg) might be due to in-situ aquatic methylation.

Regarding the MMHg levels in surface waters of the investigated Pyrenean lakes, the Autumn 2018 sampling campaign stands out from the other ones (**Figure 2**). Median values for $MMHg_{UF}$ in Spring 2017, Autumn 2017, Spring 2018, and Spring 2019 were respectively 0.010, 0.006, 0.011 and 0.013 ng L^{-1} while the median value in Autumn 2018 was 0.025 ng L^{-1}. A comparison of $MMHg_{UF}$ levels in Spring 2018 and Autumn 2018 reveals substantial increases in lakes Arratille (+248 %), Gentau (+360 %), Roumassot (+235 %), Bachimaña (+211 %), Coanga (+231 %), Panticosa (+583 %) and Sabocos (+216 %) and more moderate increases in most of the other studied lakes. Spring - summer algal bloom are controlling the whole biological turnover in those high-altitude and oligotrophic lakes [58], and intense bloom events might be responsible for such increase by promoting methylation processes in the sediments [29,59]. Arratille, Gentau, Roumassot, Coanga and Sabocos showed the lowest nitrate (NO_3^-) concentrations (from below LOD to 0.171 mg L^{-1}) in Autumn 2018, which can be an indicator of its removal by higher biological productivity [19,20,58,60]. In-situ methylation rates in lakes have already been linked to the trophic

393 status, with increasing eutrophication leading to increasing organic matter loading and
394 subsequent Hg methylation [22].

395 **Dissolved Gaseous Mercury (DGM) (Figure 2)**

396 Dissolved Gaseous Mercury (DGM) varied strongly, from 0.02 to 0.68 ng L^{-1} (outliers
397 excluded), and, overall, was higher than the measured DGM in other pristine areas (**Table 1**).
398 Indeed, DGM in Bolivian lakes vary from 0.001 to 0.017 ng L^{-1} in Lake Titicaca [22] and from 0.003
399 to 0.125 ng L^{-1} in Lake Uru Uru [24]. In the Lake Superior, in Canada, DGM measured in august
400 2000 was 0.020 ± 0.003 ng L^{-1} [15]. Even in the Adour Estuary, downstream to the Pyrenees, DGM
401 content was lower than in the Pyrenean Lakes with values ranging from 0.024 to 0.056 ng L^{-1} [32].
402 Finally, the DGM measured in the present study, with a median value of 0.11 ng L^{-1}, was in the
403 range of the open ocean waters [57]. DGM accounted for 25 ± 11 % of the Hg_{TOT} and sometimes
404 unexpectedly represents up to 55% of the total Hg.

405 The homogeneous iHg(II) concentrations contrasts with the high DGM levels measured
406 in the Pyreneans lakes of our study. Photoreduction is probably important in high-altitude lakes
407 from the Pyrenees. This photoreduction might be triggered by important solar radiation, and the
408 general oligotrophic state of the Pyrenean lakes, in comparison with Bolivian [22,24] or Canadian
409 lakes [28], might play a key role in this process. Indeed, organic matter is believed to have an impact
410 on Hg photoreduction, and it is worth noting that DOC concentrations exhibit low to moderate
411 values in the Pyrenean lakes (from 0.62 to 4.63 mg L^{-1}). Higher Hg photoreduction to elemental
412 Hg(0) therefore likely takes place in open water in which low to moderate DOC content has been
413 observed [57].

Table 1: Comparison of filtered and unfiltered inorganic mercury (iHg(II)), monomethylmercury (MMHg) and Dissolved Gaseous Mercury (DGM) concentrations in the subsurface water samples of the 19 studied lakes with literature data for worldwide pristine areas (oceans, boreal lakes, high altitude lakes) and local areas (freshwaters and estuary). %MMHg is calculated as the ratio between MMHg and non-gaseous Hg (MMHg + iHg(II)). %DGM is calculated as the ratio between DGM and total Hg (Hg_{TOT} = MMHg + iHg(II) + DGM). *THg, **Reactive Hg and ***Surface and Depth samples.

Reference	Location	Elevation (m asl)	Sampling period	$iHg(II)_F$ ng L^{-1}	$iHg(II)_{UF}$ ng L^{-1}	$MMHg_F$ (% $MMHg_F$) ng L^{-1}	$MMHg_{UF}$ (% $MMHg_{UF}$) ng L^{-1}	DGM (% DGM) ng L^{-1}
This Work	Central Pyrenees (France/Spain)	1640 - 2600	2017-2019	0.08 - 1.10	0.11 - 1.19	<0.003 - 0.035 (4 ± 3%)	<0.003 - 0.062 (4 ± 2%)	0.02 - 10.79 (29 ± 18%)
				median = 0.23	median = 0.38	median = 0.008	median = 0.011	median = 0.12
Fitzgerald et al. (2007) [57] (and references therein)	Equatorial Pacific Ocean				0.08 - 1.38**		<0.010 - 0.116	0.003 - 0.138
	North Pacific Ocean			0.03 - 0.39*				
	North Atlantic Ocean			0.48 ± 0.32*		0.209 ± 0.217		0.096 ± 0.062
	South Atlantic Ocean				0.58 ± 0.34*	<0.010 - 0.030		0.241 ± 0.160
Cavalheiro et al. (2016) [33]	Freshwaters (France)		2012	<0.14 - 2.10		<0.04 - 0.14		
Sharif et al. (2014) [32]	Adour Estuary (France)		2007 & 2010	0.28 - 0.59	0.40 - 2.66	0.014 - 0.054	0.018 - 0.124	0.024 - 0.056
Emmerton et al. (2018) [28]	Boreal Lakes (Canada, n=50)		2012 - 2016		0.36 - 5.33*		<0.01 - 0.344	
Bravo et al. (2017) [29]	Boreal Lakes (Sweden, n=10)***	3 - 229	2012 & 2013		0.9 - 7.3		0.2 - 2.9	
Rolfhus et al. (2003) [15]	Lake Superior (Canada/USA)	183	April 2000		0.57 ± 0.07*		0.005 ± 0.001	
			August 2000		0.47 ± 0.03*		0.008 ± 0.002	0.020 ± 0.003
Meuleman et al. (1995) [30]	Lake Baïkal (Russia)***	456	1992 & 1993	0.14 - 0.77*		0.002 - 0.038		
Malczyk and Branfireun (2015) [31]	Lake Zapotlán (Mexico)	1497	2007 & 2008	0.5 - 2.4*	0.9 - 10.7*	0.006 - 0.119		
Marusczak et al. (2011) [55]	Lake (Alps, n=4)	1648 - 2448	2008		<0.1 - 3.12*		0.002 - 0.005	
Alanoca et al. (2016) [24]	Uru Uru Lake (Bolivia)	3686	2010 & 2011	0.7 - 6.3	0.2 - 2.5	0.2 - 3.8	0.2 - 4.5	0.003 - 0.125
Guédron et al. (2017) [22]	Lake Titicaca	3809	2013 & 2015	0.10 - 0.82*	0.08 - 1.81*	0.003 - 0.243	0.013 - 0.306	0.001 – 0.017

420

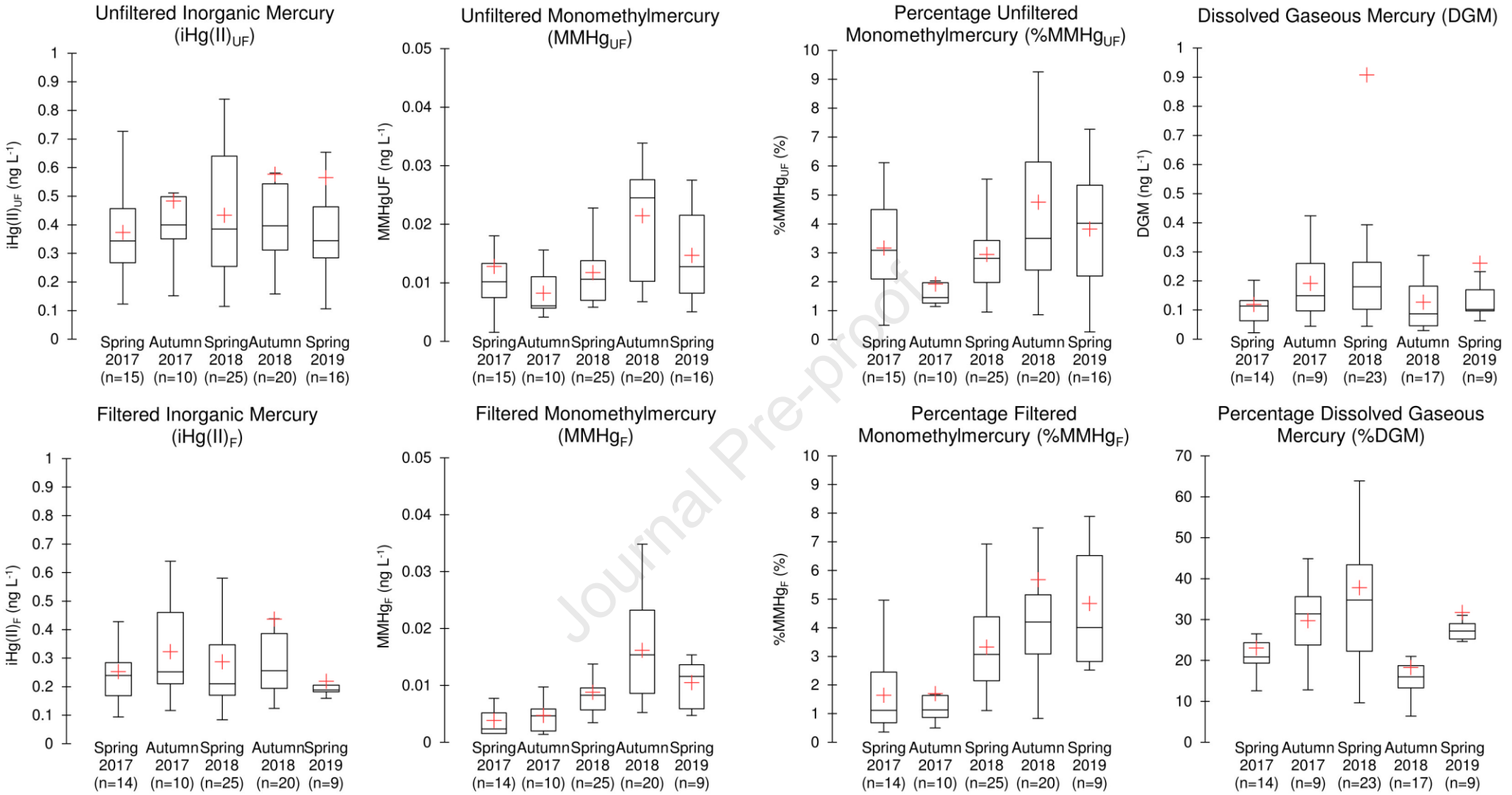

Figure 2: Boxplot representations of unfiltered and filtered iHg(II), MMHg and percentage of MMHg (calculated as the ratio between MMHg and non-gaseous Hg (MMHg + iHg(II))), and DGM and percentage of DGM (calculated as the ratio between DGM and total Hg (Hg_{TOT} = MMHg + iHg(II) + DGM)) in subsurface water samples of the 19 studied lakes. Bars indicate 10th and 90th percentile, boxes indicate 25th and 75th, marks within each box are medians, and red crosses are mean. Outliers' values especially measured for DGM are included in the graphic presentations (**see Appendix 2**).

3.2.2. Mercury compounds distribution in the water column of selected alpine lakes

Figure 3 (Lake Gentau) and **Figure 4** (Lake Sabocos) display some physico-chemical parameters, including temperature, dissolved oxygen saturation (not corrected from altitude), chlorophyll-a, TOC, Silicate, SO_4^{2-}, Cl^- and NO_3^- that might be useful to understand the distribution of mercury species (iHg(II), MMHg and DGM) in the water column of these two different lakes intensively monitored during June 2018, October 2018 and June 2019. The results are also summarised in **Table A4**. Non stratified and shallow Lakes Arratille and Azul depth profiles (**respectively Figure A5 and Figure A6)** are described in **Appendix 3**.

Lake Gentau (Figure 3)

The water column of Lake Gentau was stratified in the three sampling campaigns (June 2018, October 2018, and June 2019). Indeed, this lake is divided in three various sections: epilimnion, metalimnion, and hypolimnion, all along the year except during the short overturn spring and autumn periods [61]. In addition to the oxygen chemocline (located around 7m depth in June 2018, 10m depth in October 2018 and 8m in June 2019), Gentau also presented a thermocline in the June 2018 sampling campaign (at 10m depth), which was here not matching the depth of the chemocline.

The highest iHg(II) concentrations, either unfiltered or filtered, were detected at the deepest sampling point of the lake in June (0.75 and 0.66 ng L^{-1} in unfiltered and filtered samples, respectively) and October 2018 (0.39 and 0.36 ng L^{-1} in unfiltered and filtered samples, respectively). In June 2019, the surface water samples were characterized by the highest iHg(II) concentrations (0.27 and 0.18 ng L^{-1} in unfiltered and filtered samples, respectively). *Bravo et al.* [29] have shown that the highest total mercury concentrations in river stream systems were associated with important terrestrial DOM (Dissolved Organic Matter) and low nutrient content. In our study, TOC was low and relatively constant all along the water column during the three sampling campaigns (1.1 ± 0.3 mg L^{-1} in June 2018, 1.5 ± 0.2 mg L^{-1} in October 2018, and 1.2 ± 0.1 mg L^{-1} in June 2019). In addition, nitrate (NO_3^-), indicator of the biological productivity, decreased with depth in June 2018 (0.18 to 0.08 mg L^{-1}) while it increased with depth in October

2018 (<0.06 to 0.14 mg L^{-1}), exhibiting the seasonal changes in primary productivity and water column remineralisation of nitrogen. Also, the important increase observed for iHg(II) in the deepest point of the lake in June and October 2018 is probably due to some inputs of iHg(II) at the water-sediment interface.

MMHg concentrations were significantly higher at the deepest point of the lake in comparison with the other four sampled points. Indeed, while unfiltered and filtered MMHg in the water column in June 2018 varied from 0.008 to 0.057 ng L^{-1} and 0.006 to 0.023 ng L^{-1} respectively, MMHg unfiltered and filtered levels were respectively 0.426 and 0.318 ng L^{-1} at 18 m depth. In October 2019, the same trend was observed for MMHg: unfiltered and filtered MMHg varied from 0.027 to 0.055 ng L^{-1} and 0.011 to 0.026 ng L^{-1}, respectively, while the deepest sampled point (17m depth) exhibited MMHg levels as high as 0.388 and 0.341 ng L^{-1} for the unfiltered and filtered samples. In June 2019, unfiltered and filtered MMHg concentrations varied from 0.007 to 0.059 ng L^{-1} and <0.004 to 0.019 ng L^{-1} respectively, while it reached 0.236 and 0.157 ng L^{-1} at the deepest sampling point (17.5m depth). Moreover, MMHg represents a higher fraction of the non-gaseous Hg species (MMHg and iHg(II)) at the deepest sampled point, from 36 to 56% for unfiltered MMHg and from 32 to 60% for filtered MMHg. Anoxic conditions observed in the deepest point of Lake Gentau can host anaerobic microbial activities responsible of in-situ Hg biotic methylation in both water and surface sediments [49]. Such anoxic conditions may not be permanent in those lakes but last for several months and affect MMHg burden in lake waters. Oxygen complete consumption in bottom waters is related to both dark respiration during the ice cover in winter/spring time and also to the “Bowl-shape” - basins (Gentau, Sabocos) in which the organic deposits from the whole lake will rapidly consume bottom waters oxygen between two vertical mixing events.

Finally, vertical distribution of DGM in Gentau was quite simple with a constant and progressive decrease from surface waters (10.79 ng L^{-1} in June 2018; 0.06 ng L^{-1} in October 2018; 0.10 ng L^{-1} in June 2019) to the deepest sampled point (0.14 ng L^{-1} in June 2018 at 18m depth; 0.03 ng L^{-1} in October 2018 at 17m depth; 0.01 ng L^{-1} in June 2019 at 17.5m depth). DGM concentrations were also lower in October 2018 than in June 2018 and 2019 all along the water column. This supports the previous assumption regarding the importance of photoreduction processes in those high-altitude lakes, induced by significant solar radiation on surface waters.

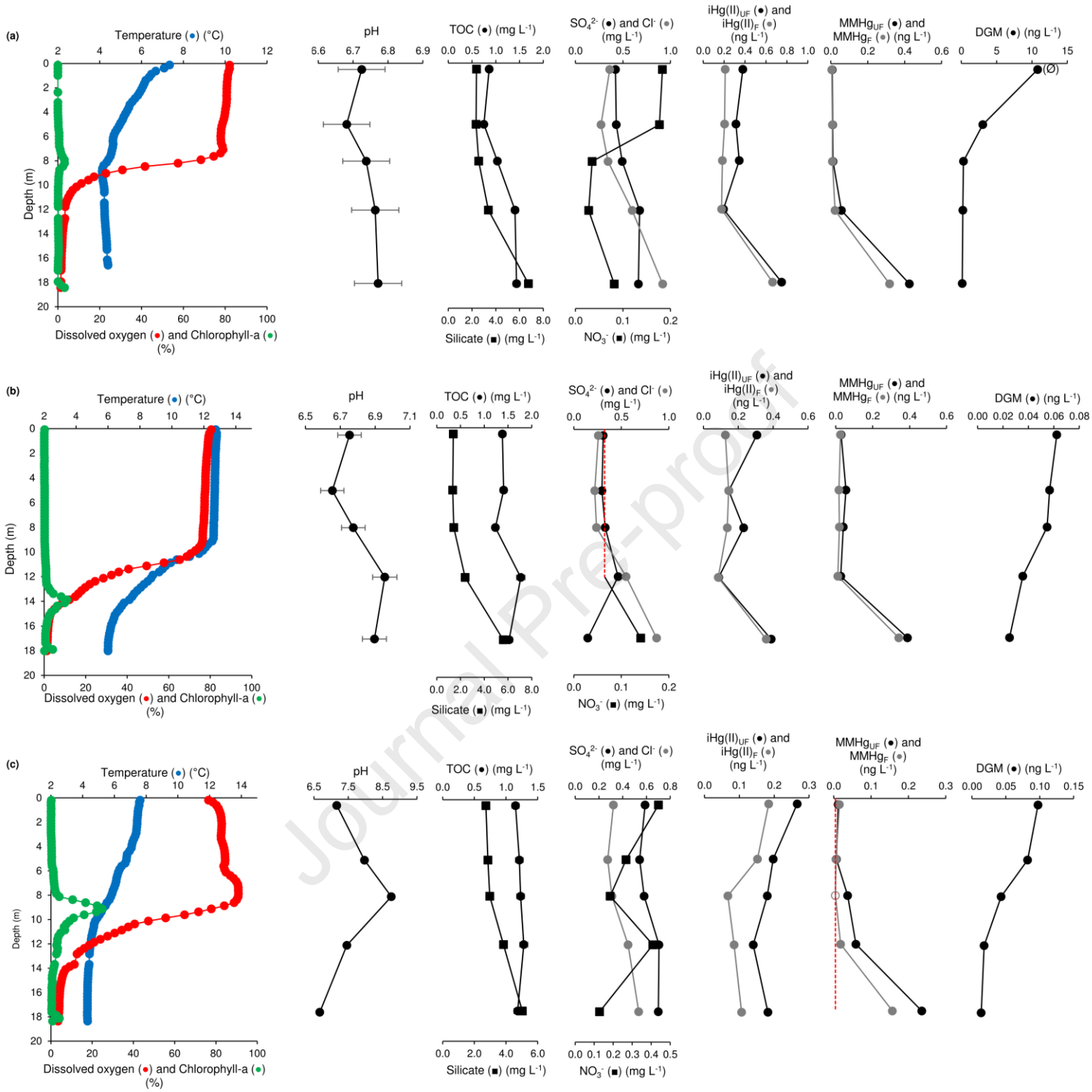

505

Figure 3: Depth profiles of temperature, percentage of dissolved oxygen saturation, chlorophyll-a (RFU) and some other chemical parameters including mercury speciation obtained in (a) June 2018, (b) October 2018 and (c) June 2019 in Lake Gentau. Red dot points correspond to the LoD. Ø correspond to outlier data for DGM in surface water (Grubbs's test; **see Table A3**).

508

509

Lake Sabocos (Figure 4)

Lake Sabocos is less stratified than Lake Gentau, but oxygen and temperature varied strongly along the water column with depletion of both physico-chemical parameters with depth, leading to almost anoxic conditions in the bottom part of this lake. Indeed, dissolved oxygen varied from 96 to 1% in June 2018, from 79 to 2% in October 2018 and from 84 to 5% in June 2019, and the chemocline, where dissolved oxygen starts decreasing, was located at 4, 10 and 5m in June 2018, October 2018, and June 2019, respectively. The thermocline was located at the same depths than chemocline and temperature varied from 17 to 5°C in June 2018, 11 to 6°C in October 2018 and 12 to 5°C in June 2019. This lake has also one specificity: it is the only one classified as an alkaline lake with pH values ranging from 7.47 to 7.71 in the surface water (June and October 2018).

iHg(II), either unfiltered or filtered, strongly varied all along the water column in the three sampling campaigns (respectively from 0.39 to 1.29 ng L^{-1} and from 0.29 to 0.53 ng L^{-1} in June 2018; from 0.53 to 0.90 ng L^{-1} and from 0.17 to 0.68 ng L^{-1} in October 2018; from 0.08 to 0.34 ng L^{-1} and from 0.02 to 0.21 ng L^{-1} in June 2019). There is no evidence for any specific trend in the iHg(II) distribution in the Lake Sabocos but the strong variations suggest that important Hg species transformations may occur.

MMHg depth profiles in Lake Sabocos indicate potential in-situ methylation with the highest MMHg levels measured in the deepest part of the lake where the oxygen level was the lowest. MMHg concentrations in unfiltered et filtered waters were respectively 0.060 and 0.025 ng L^{-1} (10 and 7% of the non-gaseous Hg), and 0.052 and 0.021 ng L^{-1} (25 and 42% of the non-gaseous Hg) in June 2018 and 2019. Increase of MMHg levels was not observed in October 2018. During this sampling campaign, no maximum of chlorophyll was detected in the water column, probably indicating a lower biological production.

Regarding the DGM concentrations, the high levels measured in surface waters in both June 2018 and 2019 (4.65 and 1.34 ng L^{-1} respectively), in comparison with deepest samples (0.56 and 0.06 ng L^{-1} respectively), is consistent with intense photoreduction enhanced during spring conditions.

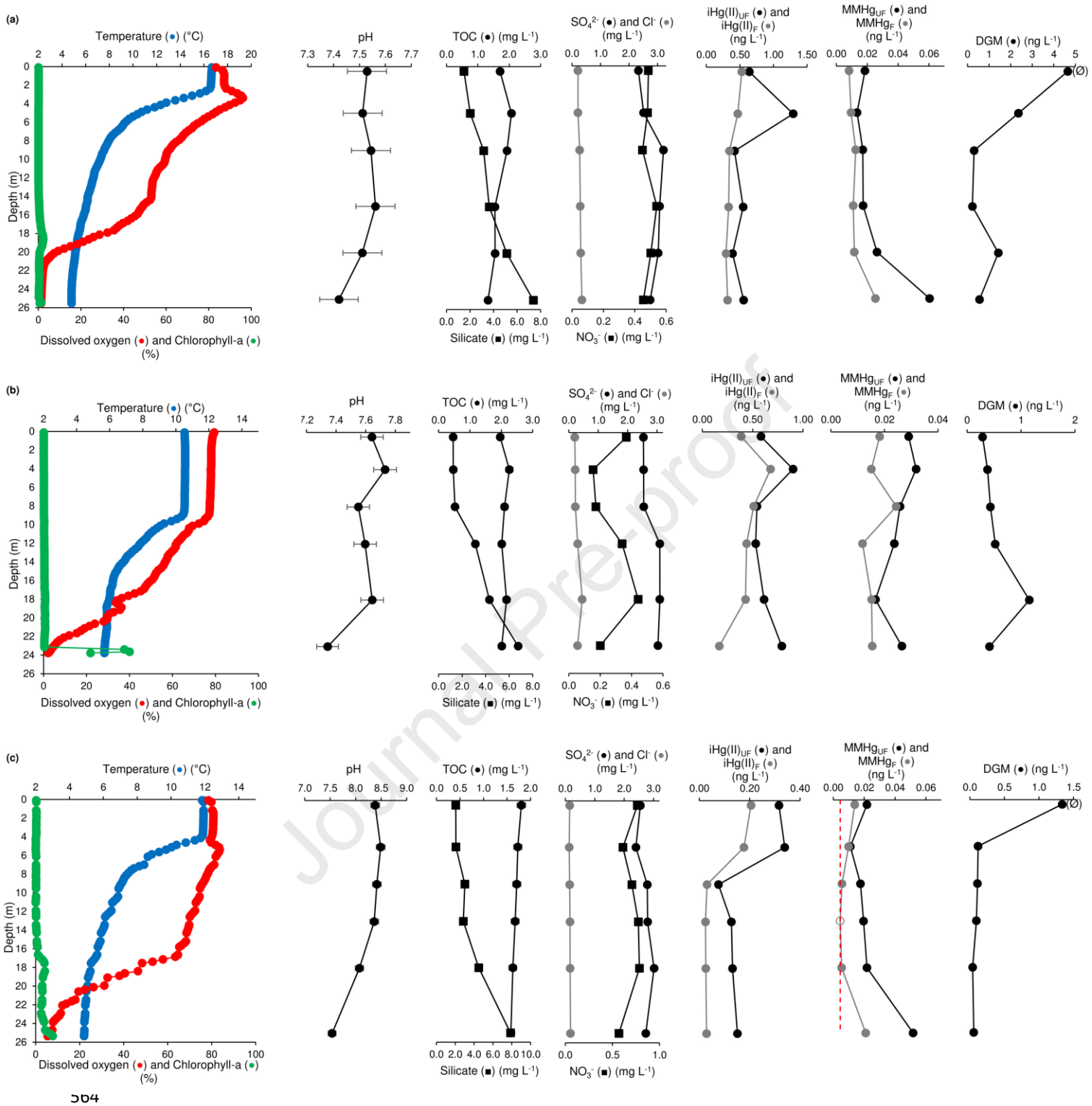

564

Figure 4: Depth profiles of temperature, percentage of dissolved oxygen saturation, chlorophyll-a (RFU) and some other chemical parameters including mercury speciation obtained in (a) June 2018, (b) October 2018 and (c) June 2019 in Lake Sabocos. Red dot points correspond to the LoD. Ø correspond to outlier data for DGM in surface water (Grubbs's test; **see Table A3**).

567

3.3. Mercury species transformations and volatilization in the water column of selected alpine lakes

Hg species incubation experiments were conducted in lakes Gentau, Sabocos and Arratille as described in **Section 2.5**, to quantify the importance of the Hg species transformations occurring in these high-altitude lakes. The obtained results are summarized in **Table 2,** together with transformation rates obtained in previous studies.

3.3.1. Methylation and Demethylation pathways

Inorganic mercury Methylation

Methylation potentials under dark and diurnal conditions obtained in unfiltered water samples ranged between <0.03 and 6.97 % day^{-1} in Lake Gentau, between <0.03 and 0.95 % day^{-1} in Lake Sabocos, and between <0.03 and 0.44 % day^{-1} in Lake Arratille (**Table 2)**. These methylation potentials are in agreement with data obtained for water samples in Canadian lakes[26], high-altitude Bolivian lakes [24] and for marine and coastal waters [32,47] using similar experimental methods. The highest methylation potentials have been measured under dark conditions in the bottom anoxic zone for Lake Gentau which exhibit 4.34 ± 0.40 % day^{-1} in June 2018, 6.97 ± 0.44 % day^{-1} in October 2018 and 1.63 ± 0.11 % day^{-1} in June 2019. For Lake Sabocos methylation is 0.81 ± 0.33 % day^{-1} in June 2018, 0.95 ± 0.38 % day^{-1} in October 2018 and 0.63 ± 0.28 % day^{-1} in June 2019. No significant difference was observed for methylation potentials for incubation performed under dark or diurnal conditions, confirming that light induced methylation is not significant in those high-altitude pristine lakes. These results also support depth profile measurements and demonstrate that reducing conditions, especially in stratified anoxic waters, promote Hg methylation due to methylating anaerobic bacteria.

Lower but measurable methylation extent were determined in the oxic subsurface waters of Lake Gentau with 0.42 ± 0.12 % day^{-1} under diurnal conditions and 0.40 ± 0.17 % day^{-1} under dark conditions in June 2018, and 0.21 ± 0.17 % day^{-1} under diurnal conditions in June 2019. In Lake Sabocos, surface water methylation was 0.09 ± 0.05 % day^{-1} under diurnal conditions and 0.26 ± 0.02 % day^{-1} under dark conditions in June 2018, and 0.34 ± 0.25 % day^{-1} under diurnal conditions and 0.17 ± 0.07 % day^{-1} under dark conditions in October 2018. Lake Arratille exhibit

596 methylation potential of 0.44 ± 0.04 % day^{-1} under diurnal conditions in June 2018. The formation
597 of MMHg in the oxic freshwater column is not fully understood yet. A recent work conducted in
598 Lake Geneva highlights that particles sinking through oxygenated water column can be
599 responsible for the production of MMHg [27]. In our study, although the methylation rates measured
600 remain low, it is measurable and suggests that reducing conditions occurring in particles
601 microenvironment within the oxic layer could also play a role.
602
603 **MMHg Demethylation**
604 Significant demethylation potentials were measured in the subsurface waters of Lake
605 Gentau (23.8 ± 4.4 % day^{-1} in June 2018; 23.9 ± 2.9 % day^{-1} in October 2018 and 35.6 ± 2.2 %
606 day^{-1} in June 2019) and Lake Sabocos (35.2 ± 9.7 % day^{-1} in June 2018; 9.0 ± 0.5 % day^{-1} in
607 October 2018 and 12.4 ± 4.2 % day^{-1} in June 2019) only at daylight conditions. These important
608 demethylation potentials have been observed in previous studies and were associated to both
609 abiotic and biotic processes [32,49]. In our study, demethylation under dark conditions was detected
610 only in Lake Sabocos within the oxicline in June 2019 (6.8 ± 4.7 % day^{-1}), while in other lakes and
611 season dark demethylation was always below 4 % day^{-1}. Therefore, our results suggest that in
612 high-altitude pristine lakes, direct light-induced photochemical demethylation in UV exposed
613 surface waters is the most significant pathway that contributes to control the extent of MMHg in
614 the water column [23].
615 Lake Sabocos exhibited an interesting result regarding the middle depth (9m), only
616 studied in June 2019. While in Lake Gentau significant demethylation was measured at the middle
617 depth of the lake (8m) in June 2018 (13.6 ± 1.2 % day^{-1}) and June 2019 (13.6 ± 0.4 % day^{-1}) only
618 under diurnal conditions and in lower extent than for the subsurface, Lake Sabocos exhibited
619 significant demethylation at both diurnal and dark conditions in June 2019 (8.2 ± 3.9 % day^{-1} and
620 6.8 ± 4.7 % day^{-1} respectively). Thus, in both stratified lakes, demethylation occurred within the
621 oxicline and cannot be related to UV photochemical reactions (i.e., no UV light). These results
622 suggest that specific microbial activity are involved due to heterotrophic (Gentau, Sabocos) and/or
623 phototrophic (Sabocos) bacteria specifically developing at the oxycline (middle depth).
624
625

Demethylation vs total MMHg loss

As mentioned previously, demethylation, especially in subsurface waters, is important in Lake Gentau and Lake Sabocos. As a reminder, demethylation potentials calculated here correspond to the transformation of MMHg into iHg(II). In **Table 2**, in addition to the demethylation potentials, total loss of MMHg potential from the experimental water solution has also been determined. Total loss of MMHg correspond to the decrease of MMHg during the incubation and could be connected to both the transformation of MMHg into iHg(II), and the transformation of MMHg into Hg(0) or other precipitated insoluble forms. The linear regression between both MMHg degradation processes (excluding middle depth dark conditions of Lake Sabocos, June 2019) exhibits a very good coefficient of determination (R^2 = 0.97; linear trend MMHg Loss = (1.7 ± 0.1) × Demethylation) (**Figure A7**). The covariation of both calculated potentials (demethylation and loss of MMHg) suggests that similar pathways occur during the different incubation experiments. These results demonstrate that a significant fraction (always below 50%) of the degraded MMHg, not recovered as soluble iHg(II), is converted to Hg(0) (reductive (photo)demethylation) or to insoluble Hg forms as final products.

Hg Net methylation assessment

In anoxic waters, the net methylation assessment (**Table 2**) allows to exhibit a potential significant production of MMHg in the bottom part of Lake Gentau with 3.25 ± 0.30 ng L^{-1} day^{-1} in June 2018, 2.71 ± 0.17 ng L^{-1} day^{-1} in October 2018, and 0.29 ± 0.02 ng L^{-1} day^{-1} in June 2019. While lower ones are determined in Lake Sabocos with 0.45 ± 0.19 ng L^{-1} day^{-1} in June 2018, 0.75 ± 0.30 ng L^{-1} day^{-1} in October 2018, and 0.09 ± 0.04 ng L^{-1} day^{-1} in June 2019. On the one hand, at the subsurface, low potential production of MMHg was observed in Lake Arratille with net methylation of 0.07 ± 0.01 ng L^{-1} day^{-1} (diurnal condition) and 0.07 ± 0.04 ng L^{-1} day^{-1} (dark condition) in June 2018. On the other hand, under diurnal conditions, the subsurface waters of Lake Gentau and Lake Sabocos behave as a sink of MMHg, as net methylation remains negative and varies from -0.01 ± 0.09 to -0.64 ± 0.08 ng L^{-1} day^{-1}.

3.3.2. Reduction and volatilization from alpine lakes

Reduction and Volatilization Flux Density in selected alpine lakes (Arratille, Gentau and Sabocos)

High iHg(II) reduction potentials (**Table 2**) were measured under diurnal conditions in subsurface waters of Lake Gentau (81.2 ± 0.8 % day^{-1} in June 2018; 20.8 ± 0.1 % day^{-1} in October 2018 and 16.9 ± 0.1 % day^{-1} in June 2019) and Lake Sabocos (13.2 % day^{-1} in June 2019), and were less significant in subsurface waters of Lake Arratille (17.3 ± 2.9 % day^{-1} in June 2018; 2.8 ± 0.2 % day^{-1} in October 2018), but still remained among the highest in comparison to previous studies [24,32,47]. These important reduction potentials are consistent with the high DGM concentrations measured, especially in Lakes Gentau and Sabocos. Regarding the dark conditions, reduction potentials at subsurface waters were detected at lower extents only in June 2018 (9.1 ± 2.6 % day^{-1}) and October 2018 (1.7 ± 0.1 % day^{-1}) for Lake Gentau, June 2019 (3.5 ± 0.1 % day^{-1}) for Lake Sabocos. Therefore, intense UV light occurring in surface waters of high-altitude lakes promotes Hg reduction.

Using the reduction potentials and the non-gaseous Hg measured at the subsurface waters, we can estimate the amount of Hg reduced per day within the first meter depth under diurnal conditions and compare it with the Volatilization Flux Density (FD) calculated as described in **Section 2.6**. All the fluxes calculated are gathered in **Table A3**.

In Lake Gentau, the amount of Hg reduced per day was 473 ± 5 ng m^{-2} day^{-1} in June 2018, 54 ± 1 ng m^{-2} day^{-1} in October 2018 and 47 ± 1 ng m^{-2} day^{-1} in June 2019. Median values of Volatilization FD in Lake Gentau were in the same order of magnitude with 48 ng m^{-2} day^{-1} for 1 m s^{-1} wind speed (from 12 to 143 ng m^{-2} day^{-1}) and 72 ng m^{-2} day^{-1} for 3 m s^{-1} wind speed (from 18 to 216 ng m^{-2} day^{-1}) (n=10). For Lake Sabocos, the quantity of Hg reduced per day was in the same range than Lake Gentau with 46 ± 1 ng m^{-2} day^{-1} in June 2019, and in the same order of magnitude than the Volatilization FD median values, 121 ng m^{-2} day^{-1} for 1 m s^{-1} wind speed (from 31 to 288 ng m^{-2} day^{-1}) and 184 ng m^{-2} day^{-1} for 3 m s^{-1} wind speed (from 46 to 436 ng m^{-2} day^{-1}) (n=4). In these two lakes, even if the Volatilization FD median values are not significantly different from the extent of Hg reduced per day, the overall range remains important. The amount of Hg reduced in Lake Arratille was lower than the other two lakes with 31 ± 5 ng m^{-2} day^{-1} in June 2018 and 14 ± 1 ng m^{-2} day^{-1} in October 2018, which is also similar to the Volatilization FD calculated

(from 20 to 178 ng m^{-2} day^{-1} for 1 m s^{-1} wind speed and from 30 to 270 ng m^{-2} day^{-1} for 3 m s^{-1} wind speed (n=7)). Overall, the gaseous Hg evasion estimated from the first meter of the water column (subsurface) represents a similar extent than the reduction potential obtained from our incubation experiments. Our results strongly support that UV light induced in-situ reduction is a major pathway controlling significant volatilization of Hg from these alpine lakes.

Volatilization Flux Density (FD) in all the studied lakes and comparison with other fluxes

Median values of Volatilization FD in all the lakes (except Arratille, Sabocos and Gentau discussed below) were 60 ng m^{-2} day^{-1} for 1 m s^{-1} wind speed (from 7 to 375 ng m^{-2} day^{-1}) and 92 ng m^{-2} day^{-1} for 3 m s^{-1} wind speed (from 11 to 568 ng m^{-2} day^{-1}). Volatilization FD did not vary strongly depending on the sampling campaign with median values from 45 to 111 ng m^{-2} day^{-1} (1 m s^{-1}) and from 68 to 168 ng m^{-2} day^{-1} (3 m s^{-1}).

It is interesting to compare these estimated Volatilization FD with wet Hg deposition fluxes (direct input and snow-ice melt), and Hg accumulation rates in sediments. The latter is commonly used as a probe for past Hg contamination in alpine lakes and atmospheric burden.

Hg concentration in wet deposition at the peatland of Pinet (Central Pyrenees, 880m asl) was recently measured at 8.0 ± 4.6 ng L^{-1} [54]. Considering that annual precipitation is 1161 mm at Pinet peat (average for the period 2010-2013) [54] and 2000 mm at lake Marboré (Central Pyrenees, 2612 m asl) [3], the studied lakes in this work (from 1620 m asl to 2600 m asl) are subjected to 25 to 44 ng m^{-2} day^{-1} Hg inputs from wet deposition. This is well in accordance with model results of Hg deposition in the Pyrenees Region from European Monitoring and Evaluation Programme (EMEP), ranging from 33 to 49 ng m^{-2} day^{-1} (Website. http://www.emep.int/). The median Volatilization FD calculated in this work are 60 to 92 ng m^{-2} day^{-1} (1 and 3 m s^{-1} wind speed, respectively) which is slightly above the maximum wet deposition. Nevertheless, considering the surface of the studied lakes the median Volatilization Flux Density can be estimated to be 2 to 3 mg day^{-1}, while considering the surface of the catchment the wet deposition inputs to Pyrenean high-altitude lakes can be estimated to be 45 to 79 mg day^{-1}. We conclude that Hg evasion does not constitute a major Hg loss at the catchment scale, but it will drastically affect its water column biogeochemistry.

Lake Marboré has been deeply studied [3,62,63], and one recent publication is also dedicated to the Hg in sediment cores from this lake (*Duval, PhD Thesis* [40]). In this study, the most recent sample (2004 AD) exhibits a Hg accumulation rate of 40 µg m^{-2} $year^{-1}$, which corresponds to an average daily Hg fluxes of 110 ng m^{-2} day^{-1}. This flux is in the same range as the median Volatilization Flux Density calculated with the gas exchange model.

Overall, the evasion fluxes calculated for the alpine lakes are very significant, and due to the high DGM levels measured in these lakes. It is worth noting that these estimations are made using an empirical water-air gas exchange model providing a rough estimate, and that the calculated Volatilization Flux Density corresponds to the free-ice period (negligible during ice cover). However, it is clear that the Hg deposited in bottom lake sediments will be drastically affected by DGM evasion and direct input from snow melt and runoff.

Table 2: Methylation (M), Demethylation (D), MMHg Loss (L), Net Methylation (NM) and Reduction (R) potentials (mean ± SD, n=3 for M, D, L and NM, n=2 for R) in unfiltered waters performed under varying light and dark conditions at different depths for Lakes Gentau, Sabocos and Arratille and for sampling campaigns June and October 2018 and June 2019, together with data from the literature. Detection limits are 0.03, 4, 4 and 1 % day-1 for Methylation, Demethylation, MMHg Loss and Reduction yields, respectively. n.d. is not determined.

Location	Sampling Period	Sampling Type	Incubation Time (h)	iHg(II) Methylation (%day^{-1})		MMHg Demethylation (%day^{-1})		MMHg Loss (%day^{-1})		Hg Reduction (%day^{-1})		Net Methylation (ng L^{-1} day^{-1})	
				Diurnal	Dark	Diurnal	Dark	Diurnal	Dark	Diurnal	Dark	Diurnal	Dark
Lake Gentau	June 2018	Subsurface (0.5m)	7.4	0.4 ± 0.1	0.4 ± 0.2	23.8 ± 4.4	<LOD	44.5 ± 4.4	7.8 ± 1.9	81.2 ± 0.8	9.1 ± 2.6	-0.01 ± 0.09	0.23 ± 0.10
(Central Pyrenees)		Middle Depth (8m)	8.5	<LOD	<LOD	13.6 ± 1.2	<LOD	23.3 ± 0.3	8.7 ± 3.6	19.5 ± 0.3	5.2 ± 0.6	-0.17 ± 0.01	-0.01 ± 0.09
		Bottom (17m)	8.7	n.d.	4.3 ± 0.4	n.d.	<LOD	n.d.	7.0 ± 3.3	n.d.	<LOD	n.d.	3.25 ± 0.30
	October 2018	Subsurface (0.5m)	7.2	<LOD	<LOD	23.9 ± 2.9	<LOD	41.7 ± 7.8	23.2 ± 2.8	20.8 ± 0.1	1.7 ± 0.1	-0.64 ± 0.08	<LOD
		Middle Depth (8m)	6.0	0.4 ± 0.2	0.5 ± 0.2	<LOD	<LOD	9.1 ± 7.4	<LOD	<LOD	<LOD	0.08 ± 0.05	0.11 ± 0.06
		Bottom (17m)	7.2	n.d.	7.0 ± 0.4	n.d.	<LOD	n.d.	28.9 ± 8.6	n.d.	<LOD	n.d.	2.71 ± 0.17
	June 2019	Subsurface (0.5m)	8.7	0.2 ± 0.2	<LOD	35.6 ± 2.2	<LOD	61.5 ± 7.0	<LOD	16.9 ± 0.1	<LOD	-0.43 ± 0.07	<LOD
		Middle Depth (8m)	8.5	<LOD	<LOD	13.6 ± 0.4	<LOD	31.5 ± 8.3	<LOD	3.7 ± 1.4	<LOD	-0.51 ± 0.01	<LOD
		Bottom (17m)	8.5	n.d.	1.6 ± 0.1	n.d.	<LOD	n.d.	<LOD	n.d.	<LOD	n.d.	0.29 ± 0.02
Lake Sabocos	June 2018	Subsurface (0.5m)	6.3	0.1 ± 0.0	0.3 ± 0.0	35.2 ± 9.7	<LOD	52.8 ± 15.4	<LOD	n.d.	n.d.	-0.52 ± 0.18	0.18 ± 0.01
(Central Pyrenees)		Bottom (27m)	6.3	n.d.	0.8 ± 0.3	n.d.	<LOD	n.d.	<LOD	n.d.	n.d.	n.d.	0.45 ± 0.19
	October 2018	Subsurface (0.5m)	6.3	0.3 ± 0.2	0.2 ± 0.1	9.0 ± 0.5	<LOD	12.2 ± 3.7	4.3 ± 1.7	n.d.	n.d.	-0.06 ± 0.13	0.10 ± 0.04
		Bottom (23m)	6.3	n.d.	1.0 ± 0.4	n.d.	<LOD	n.d.	<LOD	n.d.	n.d.	n.d.	0.75 ± 0.30
	June 2019	Subsurface (0.5m)	6.8	<LOD	<LOD	12.4 ± 4.2	<LOD	14.8 ± 7.5	<LOD	13.2	3.5 ± 0.1	-0.19 ± 0.06	<LOD
		Middle Depth (9m)	6.8	0.2 ± 0.2	0.1 ± 0.0	8.2 ± 3.9	6.8 ± 4.7	22.5 ± 4.6	24.7 ± 2.3	3.7 ± 0.4	2.4 ± 0.2	-0.14 ± 0.07	-0.11 ± 0.08
		Bottom (25m)	6.8	n.d.	0.6 ± 0.3	n.d.	<LOD	n.d.	<LOD	n.d.	<LOD	n.d.	0.09 ± 0.04

Table 2 (continued)

Lake Arratille (Central Pyrenees)	June 2018	Subsurface (0.5m)	6.0	0.4 ± 0.0	n.d.	<LOD	n.d.	22.6 ± 15.7	n.d.	17.3 ± 2.9	13.6 ± 0.8	0.07 ± 0.01	0.07 ± 0.04
		Middle Depth (6m)	5.3	0.4 ± 0.2	<LOD	<LOD	<LOD	16.4 ± 1.4	7.8 ± 0.6	n.d.	18.7 ± 5.4	n.d.	<LOD
	October 2018	Subsurface (0.5m)	5.3	n.d.	n.d.	n.d.	n.d.	n.d.	n.d.	2.8 ± 0.2	<LOD	n.d.	n.d.
		Bottom (12m)	6.7	n.d.	n.d.	n.d.	n.d.	n.d.	n.d.	n.d.	<LOD	n.d.	n.d.
Lake (Canada) [26]	2002	Oxycline	24		0.6 - 14.8				<12				
Mediterranean Sea [47]	2003 & 2004	Surface Water	24	<0.02 - 6.3	<0.02 - 3.8	3.3 - 24.5	<1.5 - 10.9			1.1 - 16.9	1.0 - 12.3		
Lake Moreno (Argentina) [64]	April 2007	Upper limit of metalimnion (30m depth)	72	27.3 - 50.8	15.4 - 23.5								
Arcachon Bay (France) [49]	2006 & 2007	Water column	24	<0.02 - 0.8	<0.02 - 1.1	1.8 - 11.9	1.3 - 9.0						
Adour river estuary (France) [32]	2007 & 2010	Surface Water	24	<0.01 - 0.4	<0.01 - 0.1	6.6 - 55.3	<2.0 - 22.1			4.3 - 43.5	0.3 - 14.7	-0.02 - 0.00	
Lake Uru Uru (Bolivia) [24]	2010 & 2011	Surface Water	24	<0.02 - 4.9	<0.02 - 7.7	<0.02 - 21.0	<0.02 - 20.5			0.1 - 1.0		-0.11 - 0.20	-0.06 - 0.45

Implication for Hg cycling in alpine lakes and climate driven perspectives

Overall, this work focusing on the water column provides a first global picture of the Hg cycling in the high-altitude lake's ecosystems including various transformations rates measured and estimated volatilization fluxes for the first time. As an example, results obtained from Lake Gentau (**Figure 5**) allow us to estimate the fate of Hg in such stratified alpine lakes and to predict the influence of changes in the hydrological cycle, the water column stratification, and the biological productivity due to anthropogenic pressure and/or climate conditions. Indeed, important methylation (290 to 3250 ng m^{-3} day^{-1}) occurs in the deepest and anoxic zone of this lake with possible harmful impacts on the biota, while important (photo)demethylation (10 to 640 ng m^{-3} day^{-1}) and (photo)reduction (47 to 473 ng m^{-3} day^{-1}) leading to Hg evasion (50 to 75 ng m^{-2} day^{-1}) take place in the surface of the lake. Future in-depth studies must be conducted on these sentinel ecosystems to better constrain fluxes and transformations and obtain a more accurate mass balance of Hg species. Consequently, further experimental studies are clearly required to assess the effect of lake waters stratification, to quantify atmospheric deposition via direct input and snow/ice melt and to evaluate the eutrophication status and major biogeochemical changes.

Direct changes in the alpine ecosystem due to human activities (e.g. tourism, agropastoralism) or more global forcing due to climate change, have a potential effect on major drivers such as water temperature or light incidence. These effects will thus have drastic consequences on the Hg cycle at high altitude lakes that can be anticipated as follow: first, warmer conditions might increase lake water stratification and anoxic conditions in bottom waters that can promote Hg methylation by microorganisms. Such conditions can also increase both Hg (photo)reduction and evasion from surface waters to the atmosphere as we observed during this study. However large uncertainties remain in those evaluations considering that major changes are also expected with atmospheric deposition at local scale and that specific evolution of the lakes depends on their geographic and topographic situations. In this work, we addressed for the first time the importance of photoreduction on the fate of Hg through gaseous Hg evasion flux densities from alpine lakes. In addition, methylation and mainly photodemethylation extents were simultaneously measured in this work, allowing to calculate the net methylation rate to assess the net MMHg balance of these competitive pathways under different seasonal and annual conditions. These preliminary assessments provide here some first conclusions on the potential

788 effect of global or climate changing drivers on the Hg cycling and impact in those "sentinel"
789 ecosystems. However more complex features were not taken into account in this work and might
790 be involved especially during winter ice cover period, very warm summer conditions or water
791 column mixing events.
792

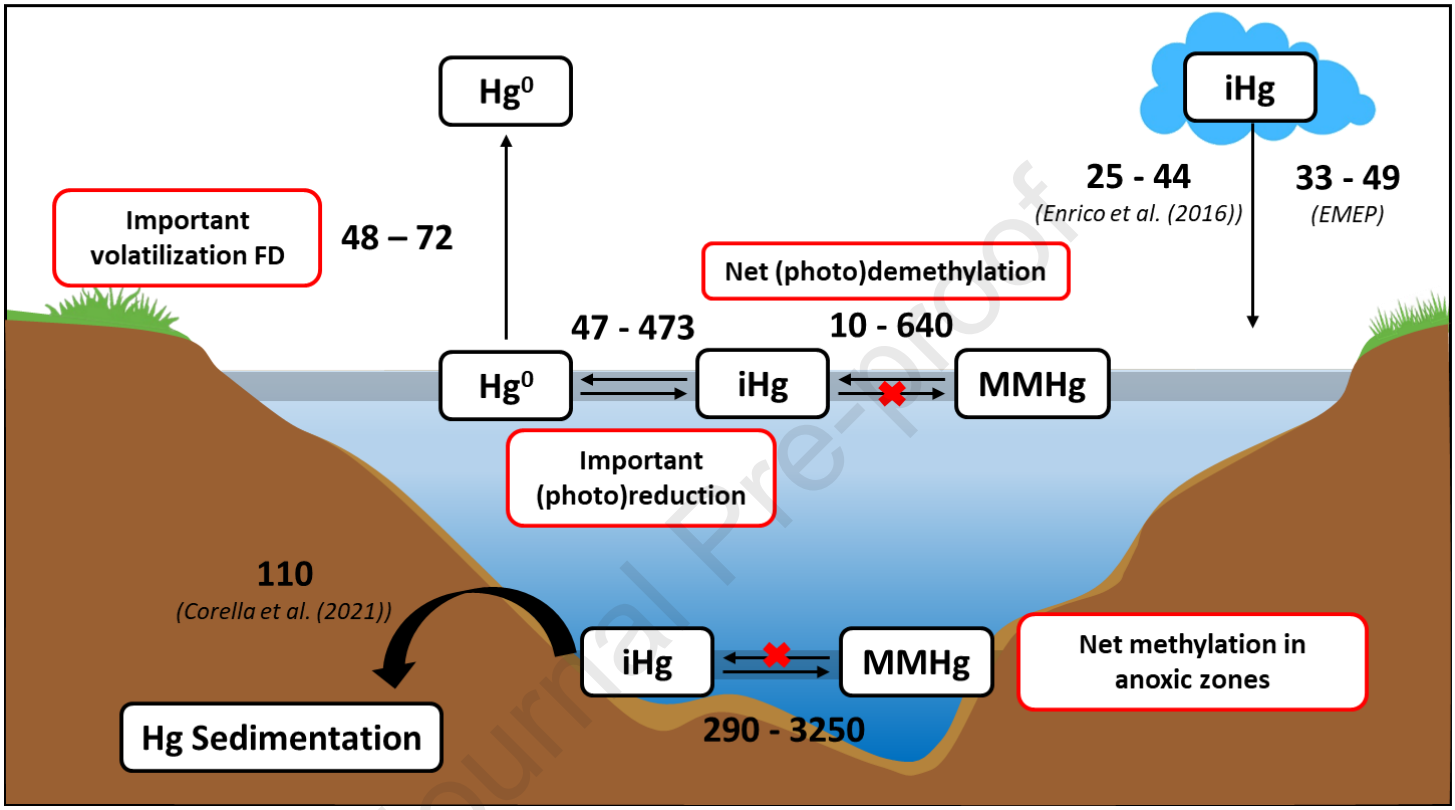

Figure 5: Hg transformations (ng m^{-3} day^{-1}) and fluxes (ng m^{-2} day^{-1}) in Lake Gentau. Red crosses are pathways not measured in this study.

793 ## Acknowledgment

794 This work has been partially supported (65%) by the FEDER funds through the INTERREG V-A
795 Spain-France-Andorra (POCTEFA 2014-2020) (REPLIM project, Ref. EFA056/15), the Spanish
796 Government (MEDLANT project CGL2016-76215-R and GECANT project CGL2017-82703-R
797 MINECO/FEDER – UE) and by the Basque Government through the Consolidated Research
798 Group Program 2013-2018 (Ref. IT-742-13). Bastien Duval is grateful to the University of the
799 Basque Country UPV/EHU for his pre-doctoral fellowship (UPV-UPPA cotutelle program).
800 Thanks to Juan Pablo Corella and Maxime Enrico for proofreading the article.
801
802

References

(1) Driscoll, C. T.; Mason, R. P.; Chan, H. M.; Jacob, D. J.; Pirrone, N. Mercury as a Global Pollutant: Sources, Pathways, and Effects. *Environmental Science & Technology* **2013**, *47* (10), 4967–4983. https://doi.org/10.1021/es305071v.

(2) Cooke, C. A.; Hintelmann, H.; Ague, J. J.; Burger, R.; Biester, H.; Sachs, J. P.; Engstrom, D. R. Use and Legacy of Mercury in the Andes. *Environmental Science & Technology* **2013**, *47* (9), 4181–4188. https://doi.org/10.1021/es3048027.

(3) Corella, J. P.; Sierra, M. J.; Garralón, A.; Millán, R.; Rodríguez-Alonso, J.; Mata, M. P.; de Vera, A. V.; Moreno, A.; González-Sampériz, P.; Duval, B.; Amouroux, D.; Vivez, P.; Cuevas, C. A.; Adame, J. A.; Wilhelm, B.; Saiz-Lopez, A.; Valero-Garcés, B. L. Recent and Historical Pollution Legacy in High Altitude Lake Marboré (Central Pyrenees): A Record of Mining and Smelting since Pre-Roman Times in the Iberian Peninsula. *Science of The Total Environment* **2021**, *751*, 141557. https://doi.org/10.1016/j.scitotenv.2020.141557.

(4) Sunderland, E. M. Mercury Exposure from Domestic and Imported Estuarine and Marine Fish in the U.S. Seafood Market. *Environmental Health Perspectives* **2007**, *115* (2), 235–242. https://doi.org/10.1289/ehp.9377.

(5) Hintelmann, H.; Keppel-Jones, K.; Evans, R. D. Constants of Mercury Methylation and Demethylation Rates in Sediments and Comparison of Tracer and Ambient Mercury Availability. *Environmental Toxicology and Chemistry* **2000**, *19* (9), 2204–2211. https://doi.org/10.1002/etc.5620190909.

(6) Selin, N. E. Global Biogeochemical Cycling of Mercury: A Review. *Annual Review of Environment and Resources* **2009**, *34* (1), 43–63. https://doi.org/10.1146/annurev.environ.051308.084314.

(7) Poulain, A. J.; Barkay, T. Cracking the Mercury Methylation Code. *Science* **2013**, *339* (6125), 1280–1281. https://doi.org/10.1126/science.1235591.

(8) Sundseth, K.; Pacyna, J. M.; Pacyna, E. G.; Munthe, J.; Belhaj, M.; Astrom, S. Economic Benefits from Decreased Mercury Emissions: Projections for 2020. *Journal of Cleaner Production* **2010**, *18* (4), 386–394. https://doi.org/10.1016/j.jclepro.2009.10.017.

(9) Ullrich, S. M.; Tanton, T. W.; Abdrashitova, S. A. Mercury in the Aquatic Environment: A Review of Factors Affecting Methylation. *Critical Reviews in Environmental Science and Technology* **2001**, *31* (3), 241–293. https://doi.org/10.1080/20016491089226.

(10) Compeau, G. C.; Bartha, R. Sulfate-Reducing Bacteria: Principal Methylators of Mercury in Anoxic Estuarine Sediment. *Appl Environ Microbiol.* **1985**, *2* (50), 498–502.

(11) Bridou, R.; Monperrus, M.; Gonzalez, P. R.; Guyoneaud, R.; Amouroux, D. Simultaneous Determination of Mercury Methylation and Demethylation Capacities of Various Sulfate-Reducing Bacteria Using Species-Specific Isotopic Tracers. *Environmental Toxicology and Chemistry* **2011**, *30* (2), 337–344. https://doi.org/10.1002/etc.395.

(12) Chételat, J. Mercury in Freshwater Ecosystems of the Canadian Arctic: Recent Advances on Its Cycling and Fate. *Science of the Total Environment* **2015**, 26.

(13) Braaten, H. F. V.; de Wit, H. A.; Fjeld, E.; Rognerud, S.; Lydersen, E.; Larssen, T. Environmental Factors Influencing Mercury Speciation in Subarctic and Boreal Lakes. *Science of The Total Environment* **2014**, *476–477*, 336–345. https://doi.org/10.1016/j.scitotenv.2014.01.030.

(14) Klapstein, S. J.; O'Driscoll, N. J. Methylmercury Biogeochemistry in Freshwater Ecosystems: A Review Focusing on DOM and Photodemethylation. *Bull Environ Contam Toxicol* **2018**, *100* (1), 14–25. https://doi.org/10.1007/s00128-017-2236-x.

(15) Rolfhus, K. R.; Sakamoto, H. E.; Cleckner, L. B.; Stoor, R. W.; Babiarz, C. L.; Back, R. C.; Manolopoulos, H.; Hurley, J. P. Distribution and Fluxes of Total and Methylmercury in Lake Superior. *Environmental Science & Technology* **2003**, *37* (5), 865–872. https://doi.org/10.1021/es026065e.

(16) Bravo, A. G.; Kothawala, D. N.; Attermeyer, K.; Tessier, E.; Bodmer, P.; Ledesma, J. L. J.; Audet, J.; Casas-Ruiz, J. P.; Catalán, N.; Cauvy-Fraunié, S.; Colls, M.; Deininger, A.; Evtimova, V. V.; Fonvielle, J. A.; Fuß, T.; Gilbert, P.; Herrero Ortega, S.; Liu, L.; Mendoza-Lera, C.; Monteiro, J.; Mor, J.-R.; Nagler, M.; Niedrist, G. H.; Nydahl, A. C.; Pastor, A.; Pegg, J.; Gutmann Roberts, C.; Pilotto, F.; Portela, A. P.; González-Quijano, C. R.; Romero, F.; Rulík, M.; Amouroux, D. The Interplay between Total Mercury, Methylmercury and Dissolved Organic Matter in Fluvial Systems: A Latitudinal

Study across Europe. *Water Research* **2018**, *144*, 172–182. https://doi.org/10.1016/j.watres.2018.06.064.

(17) Seller, P.; Kelly, C. A.; Rudd, J. W. M.; MacHutchon, A. R. Photodegradation of Methylmercury in Lakes. *Nature* **1996**, *380* (6576), 694–697. https://doi.org/10.1038/380694a0.

(18) Bouchet, S.; Tessier, E.; Masbou, J.; Point, D.; Lazzaro, X.; Monperrus, M.; Guédron, S.; Acha, D.; Amouroux, D. In Situ Photochemical Transformation of Hg Species and Associated Isotopic Fractionation in the Water Column of High-Altitude Lakes from the Bolivian Altiplano. *Environ. Sci. Technol.* **2022**, *56* (4), 2258–2268. https://doi.org/10.1021/acs.est.1c04704.

(19) Camarero, L.; Rogora, M.; Mosello, R.; Anderson, N. J.; Barbieri, A.; Botev, I.; Kernan, M.; Kopáček, J.; Korhola, A.; Lotter, A. F.; Muri, G.; Postolache, C.; Stuchlík, E.; Thies, H.; Wright, R. F. Regionalisation of Chemical Variability in European Mountain Lakes: *Regionalisation of Mountain Lakes Chemistry*. *Freshwater Biology* **2009**, *54* (12), 2452–2469. https://doi.org/10.1111/j.1365-2427.2009.02296.x.

(20) Catalan, J.; Camarero, L.; Felip, M.; Pla, S.; Ventura, M.; Buchaca, T.; Bartumeus, F.; de Mendoza, G.; Miró, A.; Casamayor, E. O.; Medina-Sánchez, J. M.; Bacardit, M.; Altuna, M.; Bartrons, M.; de Quijano, D. D. High Mountain Lakes: Extreme Habitats and Witnesses of Environmental Changes. *Limnetica* **2006**, *25* (1), 551–584. https://doi.org/10.23818/limn.25.38.

(21) Corella, J. P.; Saiz-Lopez, A.; Sierra, M. J.; Mata, M. P.; Millán, R.; Morellón, M.; Cuevas, C. A.; Moreno, A.; Valero-Garcés, B. L. Trace Metal Enrichment during the Industrial Period Recorded across an Altitudinal Transect in the Southern Central Pyrenees. *Science of The Total Environment* **2018**, *645*, 761–772. https://doi.org/10.1016/j.scitotenv.2018.07.160.

(22) Guédron, S.; Point, D.; Acha, D.; Bouchet, S.; Baya, P. A.; Tessier, E.; Monperrus, M.; Molina, C. I.; Groleau, A.; Chauvaud, L.; Thebault, J.; Amice, E.; Alanoca, L.; Duwig, C.; Uzu, G.; Lazzaro, X.; Bertrand, A.; Bertrand, S.; Barbraud, C.; Delord, K.; Gibon, F. M.; Ibanez, C.; Flores, M.; Fernandez Saavedra, P.; Ezpinoza, M. E.; Heredia, C.; Rocha, F.; Zepita, C.; Amouroux, D. Mercury Contamination Level and Speciation Inventory in Lakes Titicaca & Uru-Uru (Bolivia): Current Status and Future Trends. *Environmental Pollution* **2017**, *231*, 262–270. https://doi.org/10.1016/j.envpol.2017.08.009.

(23) Guédron, S.; Achá, D.; Bouchet, S.; Point, D.; Tessier, E.; Heredia, C.; Rocha-Lupa, S.; Fernandez-Saavedra, P.; Flores, M.; Bureau, S.; Quino-Lima, I.; Amouroux, D. Accumulation of Methylmercury in the High-Altitude Lake Uru Uru (3686 m a.s.l, Bolivia) Controlled by Sediment Efflux and Photodegradation. *Applied Sciences* **2020**, *10* (21), 7936. https://doi.org/10.3390/app10217936.

(24) Alanoca, L.; Amouroux, D.; Monperrus, M.; Tessier, E.; Goni, M.; Guyoneaud, R.; Acha, D.; Gassie, C.; Audry, S.; Garcia, M. E.; Quintanilla, J.; Point, D. Diurnal Variability and Biogeochemical Reactivity of Mercury Species in an Extreme High-Altitude Lake Ecosystem of the Bolivian Altiplano. *Environmental Science and Pollution Research* **2016**, *23* (7), 6919–6933. https://doi.org/10.1007/s11356-015-5917-1.

(25) Marusczak, N.; Larose, C.; Dommergue, A.; Paquet, S.; Beaulne, J.-S.; Maury-Brachet, R.; Lucotte, M.; Nedjai, R.; Ferrari, C. P. Mercury and Methylmercury Concentrations in High Altitude Lakes and Fish (Arctic Charr) from the French Alps Related to Watershed Characteristics. *Science of The Total Environment* **2011**, *409* (10), 1909–1915. https://doi.org/10.1016/j.scitotenv.2011.02.015.

(26) Eckley, C. S.; Hintelmann, H. Determination of Mercury Methylation Potentials in the Water Column of Lakes across Canada. *Science of The Total Environment* **2006**, *368* (1), 111–125. https://doi.org/10.1016/j.scitotenv.2005.09.042.

(27) Gascón Díez, E.; Loizeau, J.-L.; Cosio, C.; Bouchet, S.; Adatte, T.; Amouroux, D.; Bravo, A. G. Role of Settling Particles on Mercury Methylation in the Oxic Water Column of Freshwater Systems. *Environmental Science & Technology* **2016**, *50* (21), 11672–11679. https://doi.org/10.1021/acs.est.6b03260.

(28) Emmerton, C. A.; Cooke, C. A.; Wentworth, G. R.; Graydon, J. A.; Ryjkov, A.; Dastoor, A. Total Mercury and Methylmercury in Lake Water of Canada's Oil Sands Region. *Environmental Science & Technology* **2018**, *52* (19), 10946–10955. https://doi.org/10.1021/acs.est.8b01680.

(29) Bravo, A. G.; Bouchet, S.; Tolu, J.; Björn, E.; Mateos-Rivera, A.; Bertilsson, S. Molecular Composition of Organic Matter Controls Methylmercury Formation in Boreal Lakes. *Nature Communications* **2017**, *8* (1). https://doi.org/10.1038/ncomms14255.

(30) Meuleman, C.; Leermakers, M.; Baeyens, W. Mercury Speciation in Lake Baikal. *Water, Air, & Soil Pollution* **1995**, *80* (1–4), 539–551. https://doi.org/10.1007/BF01189704.

(31) Malczyk, E. A.; Branfireun, B. A. Mercury in Sediment, Water, and Fish in a Managed Tropical Wetland-Lake Ecosystem. *Science of The Total Environment* **2015**, *524–525*, 260–268. https://doi.org/10.1016/j.scitotenv.2015.04.015.

(32) Sharif, A.; Monperrus, M.; Tessier, E.; Bouchet, S.; Pinaly, H.; Rodriguez-Gonzalez, P.; Maron, P.; Amouroux, D. Fate of Mercury Species in the Coastal Plume of the Adour River Estuary (Bay of Biscay, SW France). *Science of The Total Environment* **2014**, *496*, 701–713. https://doi.org/10.1016/j.scitotenv.2014.06.116.

(33) Cavalheiro, J.; Sola, C.; Baldanza, J.; Tessier, E.; Lestremau, F.; Botta, F.; Preud'homme, H.; Monperrus, M.; Amouroux, D. Assessment of Background Concentrations of Organometallic Compounds (Methylmercury, Ethyllead and Butyl- and Phenyltin) in French Aquatic Environments. *Water Research* **2016**, *94*, 32–41. https://doi.org/10.1016/j.watres.2016.02.010.

(34) Adrian, R.; O'Reilly, C. M.; Zagarese, H.; Baines, S. B.; Hessen, D. O.; Keller, W.; Livingstone, D. M.; Sommaruga, R.; Straile, D.; Van Donk, E.; Weyhenmeyer, G. A.; Winder, M. Lakes as Sentinels of Climate Change. *Limnology and Oceanography* **2009**, *54* (6part2), 2283–2297. https://doi.org/10.4319/lo.2009.54.6_part_2.2283.

(35) UNEP. *Global Mercury Assessment 2013: Sources, Emissions, Releases and Environmental Transport*; UNEP Chemicals Branch: Geneva, Switzerland, 2013.

(36) Obrist, D.; Kirk, J. L.; Zhang, L.; Sunderland, E. M.; Jiskra, M.; Selin, N. E. A Review of Global Environmental Mercury Processes in Response to Human and Natural Perturbations: Changes of Emissions, Climate, and Land Use. *Ambio* **2018**, *47* (2), 116–140. https://doi.org/10.1007/s13280-017-1004-9.

(37) Zaharescu, D. G.; Hooda, P. S.; Burghelea, C. I.; Palanca-Soler, A. A Multiscale Framework for Deconstructing the Ecosystem Physical Template of High-Altitude Lakes. *Ecosystems* **2016**, *19* (6), 1064–1079. https://doi.org/10.1007/s10021-016-9987-9.

(38) Bueno, M.; Duval, B.; Tessier, E.; Romero-Rama, A.; Kortazar, L.; Fernandez, L. A.; De Diego, A.; Amouroux, D. Selenium Distribution and Speciation in Waters of Pristine Alpine Lakes from Central-Western Pyrenees (France-Spain). *Environ. Sci.: Processes Impacts* **2022**, 10.1039.D1EM00430A. https://doi.org/10.1039/D1EM00430A.

(39) Gascoin, S.; Grizonnet, M.; Bouchet, M.; Salgues, G.; Hagolle, O. Theia Snow Collection: High-Resolution Operational Snow Cover Maps from Sentinel-2 and Landsat-8 Data. *Earth System Science Data* **2019**, *11* (2), 493–514. https://doi.org/10.5194/essd-11-493-2019.

(40) Duval, B. Ecodynamics of Metals and Metalloids in Pyrenean Lakes in Relation to Climate Change and Anthropogenic Pressure, UPV/EHU and UPPA, 2020.

(41) Catalan, J.; Ballesteros, E.; Gacia, E.; Palau, A.; Camarero, L. Chemical Composition of Disturbed and Undisturbed High-Mountain Lakes in the Pyrenees: A Reference for Acidified Sites. *Water Research* **1993**, *27* (1), 133–141. https://doi.org/10.1016/0043-1354(93)90203-T.

(42) Camarero, L.; Catalan, J. A Simple Model of Regional Acidification for High Mountain Lakes : Application to the Pyrenean Lakes (North-East Spain). *Water Research* **1998**, *32* (4), 1126–1136. https://doi.org/10.1016/S0043-1354(97)00291-1.

(43) Camarero, L.; Bacardit, M.; de Diego, A.; Arana, G. Decadal Trends in Atmospheric Deposition in a High Elevation Station: Effects of Climate and Pollution on the Long-Range Flux of Metals and Trace Elements over SW Europe. *Atmospheric Environment* **2017**, *167*, 542–552. https://doi.org/10.1016/j.atmosenv.2017.08.049.

(44) Monperrus, M.; Tessier, E.; Veschambre, S.; Amouroux, D.; Donard, O. Simultaneous Speciation of Mercury and Butyltin Compounds in Natural Waters and Snow by Propylation and Species-Specific Isotope Dilution Mass Spectrometry Analysis. *Analytical and Bioanalytical Chemistry* **2005**, *381* (4), 854–862. https://doi.org/10.1007/s00216-004-2973-7.

(45) Amouroux, D.; Tessier, E.; Pécheyran, C.; Donard, O. F. X. Sampling and Probing Volatile Metal(Loid) Species in Natural Waters by in-Situ Purge and Cryogenic Trapping Followed by Gas Chromatography and Inductively Coupled Plasma Mass Spectrometry (P-CT–GC–ICP/MS). *Analytica Chimica Acta* **1998**, *377* (2–3), 241–254. https://doi.org/10.1016/S0003-2670(98)00425-5.

(46) Bouchet, S.; Tessier, E.; Monperrus, M.; Bridou, R.; Clavier, J.; Thouzeau, G.; Amouroux, D. Measurements of Gaseous Mercury Exchanges at the Sediment–Water, Water–Atmosphere and Sediment–Atmosphere Interfaces of a Tidal Environment (Arcachon Bay, France). *Journal of Environmental Monitoring* **2011**, *13* (5), 1351. https://doi.org/10.1039/c0em00358a.

(47) Monperrus, M.; Tessier, E.; Amouroux, D.; Leynaert, A.; Huonnic, P.; Donard, O. F. X. Mercury Methylation, Demethylation and Reduction Rates in Coastal and Marine Surface Waters of the Mediterranean Sea. *Marine Chemistry* **2007**, *107* (1), 49–63. https://doi.org/10.1016/j.marchem.2007.01.018.

(48) Rodriguez-Gonzalez, P.; Bouchet, S.; Monperrus, M.; Tessier, E.; Amouroux, D. In Situ Experiments for Element Species-Specific Environmental Reactivity of Tin and Mercury Compounds Using Isotopic Tracers and Multiple Linear Regression. *Environmental Science and Pollution Research* **2013**, *20* (3), 1269–1280. https://doi.org/10.1007/s11356-012-1019-5.

(49) Bouchet, S.; Amouroux, D.; Rodriguez-Gonzalez, P.; Tessier, E.; Monperrus, M.; Thouzeau, G.; Clavier, J.; Amice, E.; Deborde, J.; Bujan, S.; Grall, J.; Anschutz, P. MMHg Production and Export from Intertidal Sediments to the Water Column of a Tidal Lagoon (Arcachon Bay, France). *Biogeochemistry* **2013**, *114* (1–3), 341–358. https://doi.org/10.1007/s10533-012-9815-z.

(50) Fu, X.; Marusczak, N.; Wang, X.; Gheusi, F.; Sonke, J. E. Isotopic Composition of Gaseous Elemental Mercury in the Free Troposphere of the Pic Du Midi Observatory, France. *Environmental Science & Technology* **2016**, *50* (11), 5641–5650. https://doi.org/10.1021/acs.est.6b00033.

(51) Andersson, M. E.; Gårdfeldt, K.; Wängberg, I.; Strömberg, D. Determination of Henry's Law Constant for Elemental Mercury. *Chemosphere* **2008**, *73* (4), 587–592. https://doi.org/10.1016/j.chemosphere.2008.05.067.

(52) Cole, J. J.; Caraco, N. F. Atmospheric Exchange of Carbon Dioxide in a Low-Wind Oligotrophic Lake Measured by the Addition of SF_6. *Limnology and Oceanography* **1998**, *43* (4), 647–656. https://doi.org/10.4319/lo.1998.43.4.0647.

(53) Bacardit, M.; Camarero, L. Atmospherically Deposited Major and Trace Elements in the Winter Snowpack along a Gradient of Altitude in the Central Pyrenees: The Seasonal Record of Long-Range Fluxes over SW Europe. *Atmospheric Environment* **2010**, *44* (4), 582–595. https://doi.org/10.1016/j.atmosenv.2009.06.022.

(54) Enrico, M.; Roux, G. L.; Marusczak, N.; Heimbürger, L.-E.; Claustres, A.; Fu, X.; Sun, R.; Sonke, J. E. Atmospheric Mercury Transfer to Peat Bogs Dominated by Gaseous Elemental Mercury Dry Deposition. *Environmental Science & Technology* **2016**, *50* (5), 2405–2412. https://doi.org/10.1021/acs.est.5b06058.

(55) Marusczak, N.; Larose, C.; Dommergue, A.; Yumvihoze, E.; Lean, D.; Nedjai, R.; Ferrari, C. Total Mercury and Methylmercury in High Altitude Surface Snow from the French Alps. *Science of The Total Environment* **2011**, *409* (19), 3949–3954. https://doi.org/10.1016/j.scitotenv.2011.06.040.

(56) Lamborg, C. H.; Hammerschmidt, C. R.; Bowman, K. L.; Swarr, G. J.; Munson, K. M.; Ohnemus, D. C.; Lam, P. J.; Heimbürger, L.-E.; Rijkenberg, M. J. A.; Saito, M. A. A Global Ocean Inventory of Anthropogenic Mercury Based on Water Column Measurements. *Nature* **2014**, *512* (7512), 65–68. https://doi.org/10.1038/nature13563.

(57) Fitzgerald, W. F.; Lamborg, C. H.; Hammerschmidt, C. R. Marine Biogeochemical Cycling of Mercury. *Chemical Reviews* **2007**, *107* (2), 641–662. https://doi.org/10.1021/cr050353m.

(58) Santolaria, Z.; Arruebo, T.; Urieta, J. S.; Lanaja, F. J.; Pardo, A.; Matesanz, J.; Rodriguez-Casals, C. Hydrochemistry Dynamics in Remote Mountain Lakes and Its Relation to Catchment and Atmospheric Features: The Case Study of Sabocos Tarn, Pyrenees. *Environmental Science and Pollution Research* **2015**, *22* (1), 231–247. https://doi.org/10.1007/s11356-014-3310-0.

(59) Lei, P.; Nunes, L. M.; Liu, Y.-R.; Zhong, H.; Pan, K. Mechanisms of Algal Biomass Input Enhanced Microbial Hg Methylation in Lake Sediments. *Environment International* **2019**, *126*, 279–288. https://doi.org/10.1016/j.envint.2019.02.043.

(60) Camarero, L.; Catalan, J. Atmospheric Phosphorus Deposition May Cause Lakes to Revert from Phosphorus Limitation Back to Nitrogen Limitation. *Nature Communications* **2012**, *3*, 1118. https://doi.org/10.1038/ncomms2125.

(61) PNP. ETUDE PISCICOLE DES LACS D'AYOUS, 2013.

(62) Corella, J. P.; Saiz-Lopez, A.; Sierra, M. J.; Mata, M. P.; Millán, R.; Morellón, M.; Cuevas, C. A.; Moreno, A.; Valero-Garcés, B. L. Trace Metal Enrichment during the Industrial Period Recorded across an Altitudinal Transect in the Southern Central Pyrenees. *Science of The Total Environment* **2018**, *645*, 761–772. https://doi.org/10.1016/j.scitotenv.2018.07.160.

(63) Corella, J. P.; Valero-Garcés, B. L.; Wang, F.; Martínez-Cortizas, A.; Cuevas, C. A.; Saiz-Lopez, A. 700 Years Reconstruction of Mercury and Lead Atmospheric Deposition in the Pyrenees (NE Spain). *Atmospheric Environment* **2017**, *155*, 97–107. https://doi.org/10.1016/j.atmosenv.2017.02.018.

(64) Ribeiro Guevara, S.; Queimaliños, C. P.; Diéguez, M. del C.; Arribére, M. Methylmercury Production in the Water Column of an Ultraoligotrophic Lake of Northern Patagonia, Argentina. *Chemosphere* **2008**, *72* (4), 578–585. https://doi.org/10.1016/j.chemosphere.2008.03.011.

Appendices: Dynamics, distribution, and transformations of mercury species from Pyrenean high-altitude lakes

Bastien Duval[*,1,2], Emmanuel Tessier[1], Leire Kortazar[2], Luis Angel Fernandez[2], Alberto de Diego[2], David Amouroux[1]

[1]*Universite de Pau et des Pays de l'Adour / E2S UPPA, CNRS, Institut des Sciences Analytiques et de Physico-chimie pour l'Environnement et les Materiaux, UMR5254, Helioparc, 64053 Pau, France*

[2]*Kimika Analitikoa Saila, Euskal Herriko Unibertsitatea UPV/EHU, Sarriena Auzoa z/g, 48940 Leioa (Basque Country)*

**Corresponding authors*

Bastien Duval E-mail: bastien.duval@univ-pau.fr

David Amouroux E-mail: david.amouroux @univ-pau.fr

Appendix 1: Recovery of gaseous and non-volatile Hg species during sample processing

One concern drove our attention regarding the results for Hg species. Indeed, the unfiltered non-gaseous mercury, calculated as the sum of iHg(II) and MMHg, ranges from 0.11 to 3.13 ng L^{-1} in the subsurface water samples with a median value of 0.39 ng L^{-1}, while DGM can be very significant and ranges from 0.02 to 10.79 ng L^{-1} with a median value of 0.11 ng L^{-1}. As a consequence, the recovery of DGM, mainly as Hg(0) (and potentially as DMHg), in collected water samples filtration, acidification and storage is always questionable. To answer properly to that question, in the last sampling campaigns June 2019, we collected in 125 mL Teflon container the water sample that has been previously purged to collect DGM species on gold-coated sand trap. These "purged samples" were acidified adding high-purity HCl (1% v/v) (Trace metal grade) and analysed by GC-ICP-MS following the protocol described in **2. Material and Methods**. The **Figure A2** shows a comparison between results obtained in purged and unpurged unfiltered samples for both methylated (MMHg) and inorganic (iHg(II)) Hg. On the one hand, with good coefficient of determination (R^2 = 0.91) and a slope not significantly different from 1 (0.94±0.07), the results for iHg(II) analysis confirm the fact that gaseous Hg (DGM) is not a significant contributor to Hg(II) measured in unpurged samples. On the other hand, the slope obtained for the MMHg analysis is lower than 1 (R^2 = 0.98, slope = 0.75±0.02), thus suggesting that in unpurged samples some DMHg was also occurring. This was further confirmed by the detection of DMHg (<0.2 pg L^{-1}) in carbotrap columns , used in a parallel study to quantify the volatile selenium species [1,2]. Indeed, in the last depth of Lake Gentau (17.5m, anoxic zone) and in the last two depths of Lake Sabocos (18 and 25m, anoxic zone) and the middle depths of Lake Sabocos (9 and 13m, maximum chlorophyll-a, witness of algae production), DMHg was detected in the carbotrap columns. Regarding the methylated species quantified by GC-ICPMS, removing the samples exhibiting suboxic to anoxic conditions (three last depths from Gentau, 8, 12 and 17.5m; last depth from Sabocos 25m), the slope becomes not significantly different from 1 (R^2 = 0.91, slope = 0.92±0.09). Overall, in most of the cases, especially regarding subsurface samples, DMHg is negligible in comparison with MMHg, and the measured methylated species are mainly in the form of MMHg.

Appendix 2: Hg measurement outliers for Total Hg (Hg_{TOT}) and DGM

Regarding total Hg (Hg_{TOT}), defined here as the sum of concentrations of iHg(II), MMHg and DGM, in unfiltered samples (DGM only measured in unfiltered samples), seven specific samples stood out as outliers (Grubbs's tests, p-value < 0.05 then p-value = 0.063 > 0.05).

Major five outliers concern two specific and particular lakes : Lake Gentau (June 2018, 10:50 a.m.) and Lake Sabocos (June 2018, 09:45 a.m., 00:35 p.m. and 3:35 p.m.; June 2019, 00:30 p.m.). This is mainly because Lakes Gentau and Sabocos exhibited important DGM with extremely high values around midday (DGM = 10.79 ng L^{-1} in June 2018 for Lake Gentau; DGM = 4.65 ng L^{-1} in June 2018 and DGM = 1.34 ng L^{-1} in June 2019 for Lake Sabocos) when the light incidence was the highest (**Figure A4**). The explanation is not clear, but this important DGM might be due to i) accumulation of DGM under the ice cover during the winter or ii) important iHg(II) provided by the snow melt then converted into Hg(0) by reduction pathways. In both cases, it implies that the sampling has been done right after the spring period, where the lakes are frozen and the catchment is covered by snow, which is the case in June 2018. Indeed, a few days before the sampling, more than 90 % of the studied lakes were completely frozen. However, it remains difficult to explain such exceptionally high levels of DGM measured only in these two lakes. Further studies, with intensive monitoring and sampling during several days at the snowmelt period are needed to fully understand the mechanisms occurring in those Pyrenean Lakes. To avoid bias interpretation, these five samples are discarded for the discussion on DGM levels and volatilization in high-altitude lakes.

In Lake Coanga in October 2018 at 8:50 a.m., very high levels of iHg(II) were measured in both filtered ($iHg(II)_F$ = 2.68 ng L^{-1}) and unfiltered ($iHg(II)_{UF}$ = 2.88 ng L^{-1}) samples. In this sample, filtered and unfiltered MMHg and DGM does not differ strongly from the other samples suggesting that this high iHg(II), either filtered or unfiltered, might be due punctual iHg(II) inputs or simply to contamination during the sample collection: this sample will be discarded from the discussion on iHg(II), and consequently from Hg_{TOT}. In Lake Panticosa in October 2017 at 00:30 p.m., the relatively high levels of both iHg(II) ($iHg(II)_F$ = 0.64 ng L^{-1}; $iHg(II)_{UF}$ = 0.68 ng L^{-1}) and DGM (DGM = 1.21 ng L^{-1}) suggested that this specific sample was enriched in Hg, probably coming either from the catchment (the biggest one, 3229 Ha) or from punctual high Hg inputs.

Appendix 3: Mercury species distribution in the water column of Lake Arratille (Figure A5) and Lake Azul (Figure A6)

In the shallow alpine Lake Arratille (2256 m asl.), physico-chemical parameters measured in-situ with the multiparameter probe (temperature, oxygen and chorophyll) did not vary strongly within the water column. Indeed, the average temperature was 5.0 ± 0.4 °C in June 2018 and 8.0 ± 0.9 °C in October 2018, and the average dissolved oxygen was 65 ± 23 % in June 2018 and 71 ± 10 % in October 2018. Nevertheless, it is worth noting that a short decrease in both temperature and oxygen is observed in the last 2 meters of the lake in both June and October 2018. Concerning the mercury species distribution, no significant difference was observed for unfiltered and filtered iHg(II) (0.26±0.10 and 0.18±0.05 ng L^{-1}, respectively), unfiltered and filtered MMHg (0.010±0.04 and 0.008±0.03 ng L^{-1}, respectively) and DGM (0.13±0.06 ng L^{-1}) along the water column, suggesting a well-mixed lake with clear water.

In the shallower and more elevated Lake Azul (2420 m asl.), dissolved oxygen (76 ± 1 % in June 2018 and 72 ± 2 % in October 2018) and temperature (4.8 ± 0.1 °C in June 2018 and 5.1 ± 0.2 °C in October 2018) did not vary at all along the water column. Regarding Hg species, on the one hand, no specific trend was observed in June 2018 for unfiltered and filtered iHg(II) (0.36±0.05 and 0.30±0.02 ng L^{-1}, respectively) unfiltered and filtered MMHg (0.006±0.001 and 0.004±0.001 ng L^{-1}, respectively) and DGM (0.12±0.04 ng L^{-1}). On the other hand, a significant increase was observed with depth in October 2018 for all Hg compounds, probably as a result of sediment punctual remobilisation of Hg.

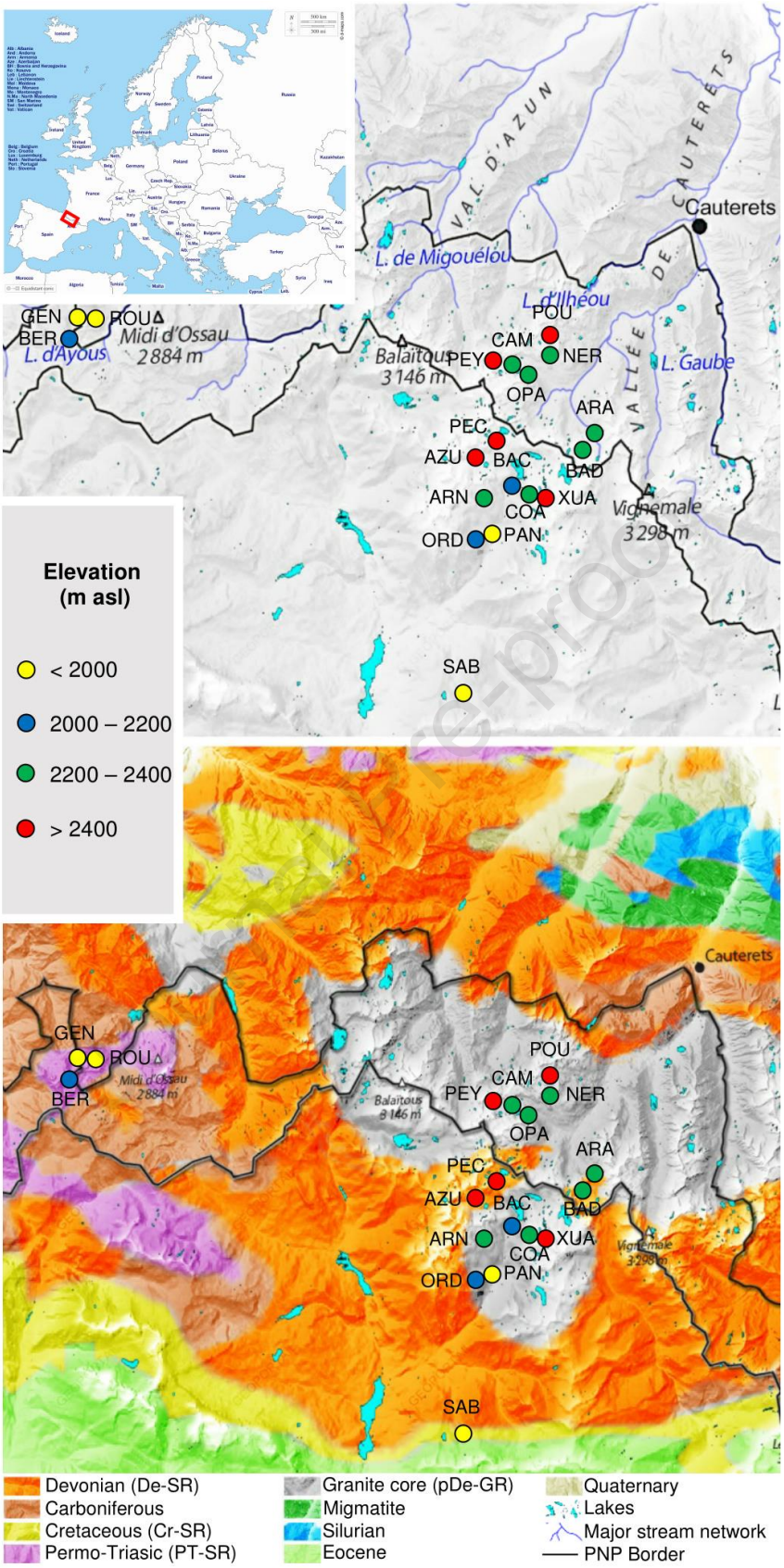

Figure A1: Studied lakes together with geology of their catchments (adapted with permission from *Zaharescu et al.*[3]); circles show position of the lakes, and colors indicate the elevation of the corresponding lakes. Lake acronyms are detailed in **Table A1**.

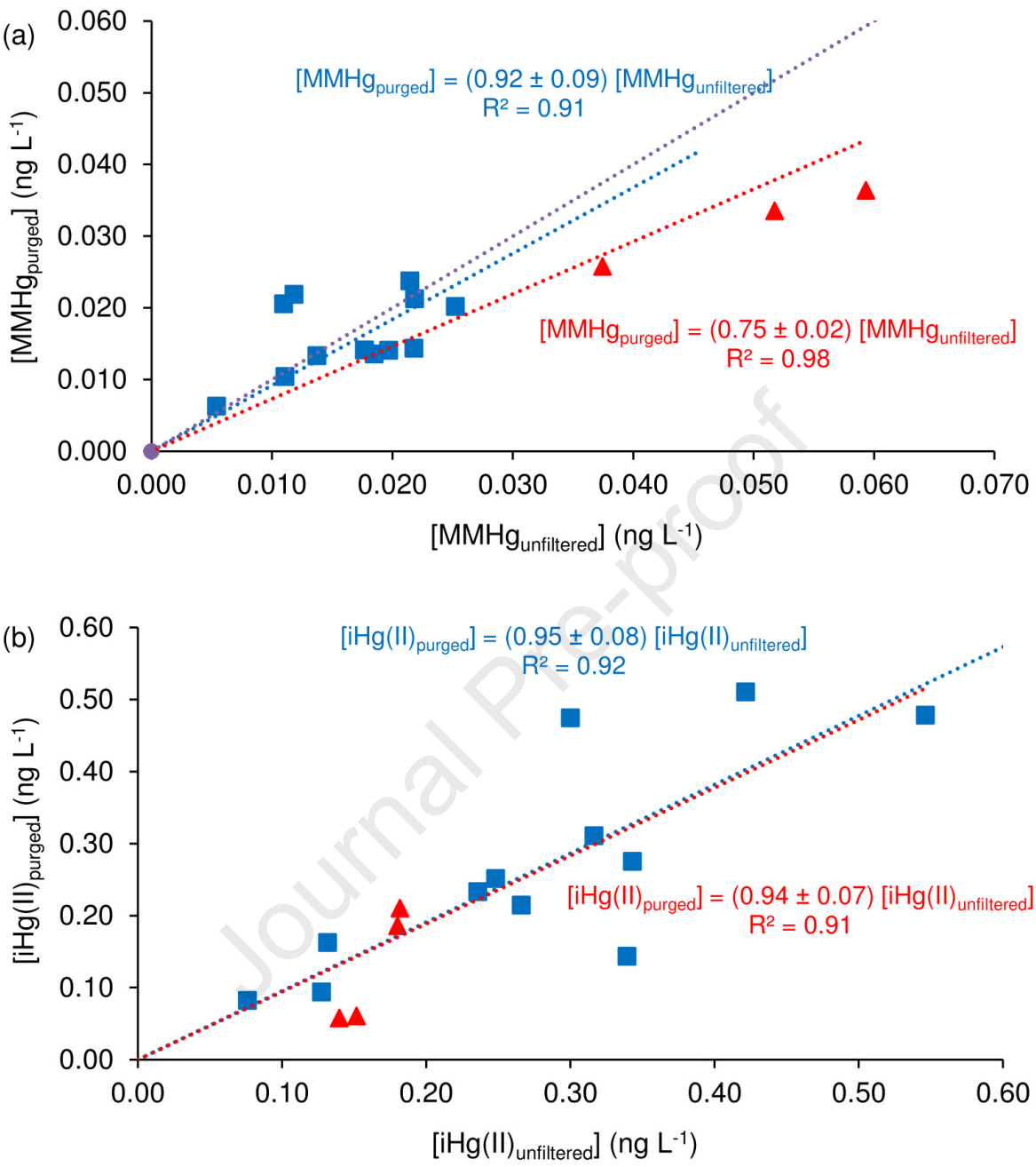

Figure A2: Comparison of (a) MMHg concentrations (ng L^{-1}) obtained in purged and unfiltered samples (last Lake Gentau depth not shown) and (b) iHg(II) concentrations (ng L^{-1}) obtained in purged and unfiltered samples for June 2019 sampling campaign. Square blue points correspond to samples collected in well oxygenated depths (oxic water) while triangle red points correspond to samples collected in not well oxygenated depths (anoxic water). Red dashed line is the linear regression using all the samples while blue dashed line included only samples from oxic water.

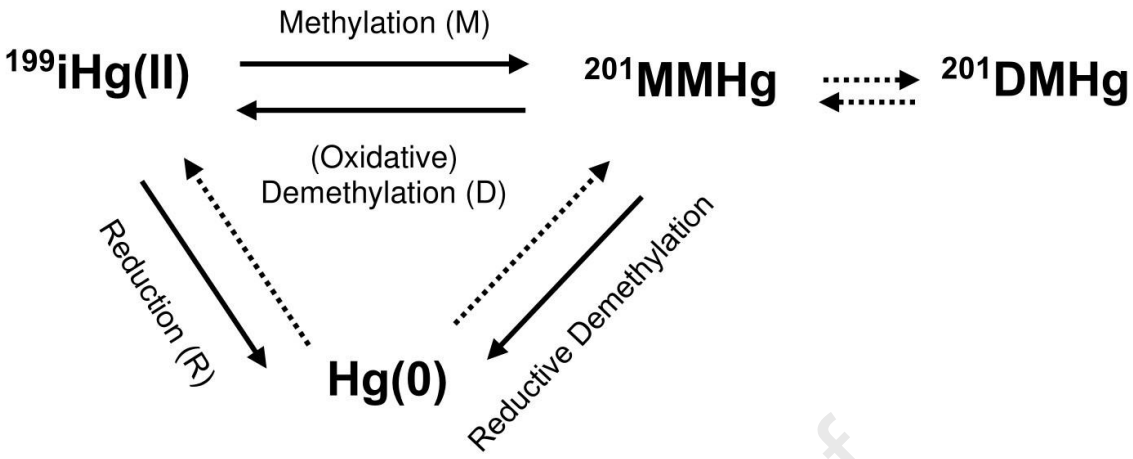

Figure A3: Reactivity model of Hg compounds. Solid arrows correspond to the reaction pathways that can be calculated with the incubation experiments, and dotted arrows the pathways that cannot be quantified. MMHg Loss is calculated as the sum of Oxidative and Reductive Demethylation.

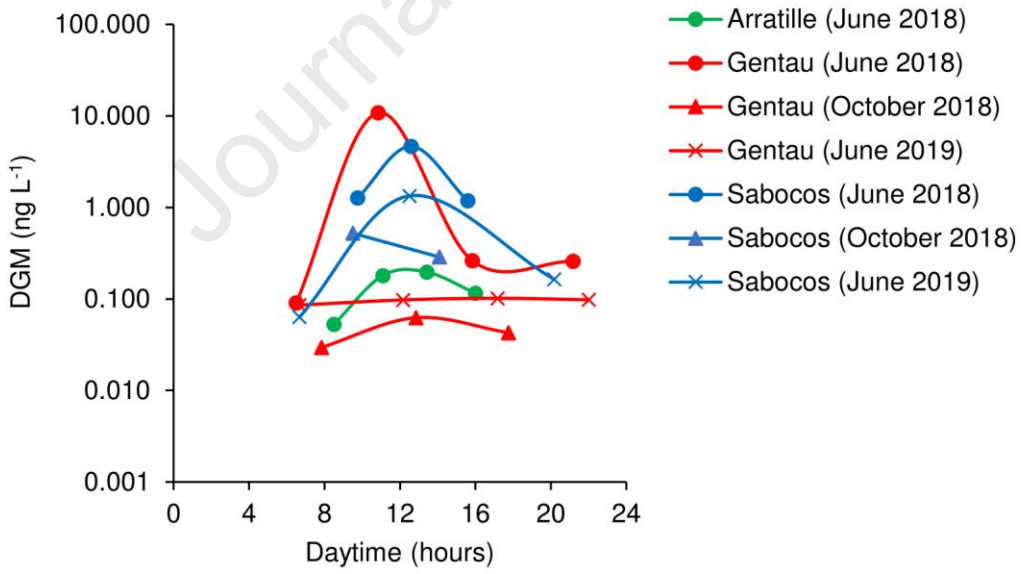

Figure A4: Daily variation of DGM in Lakes Arratille, Gentau and Sabocos.

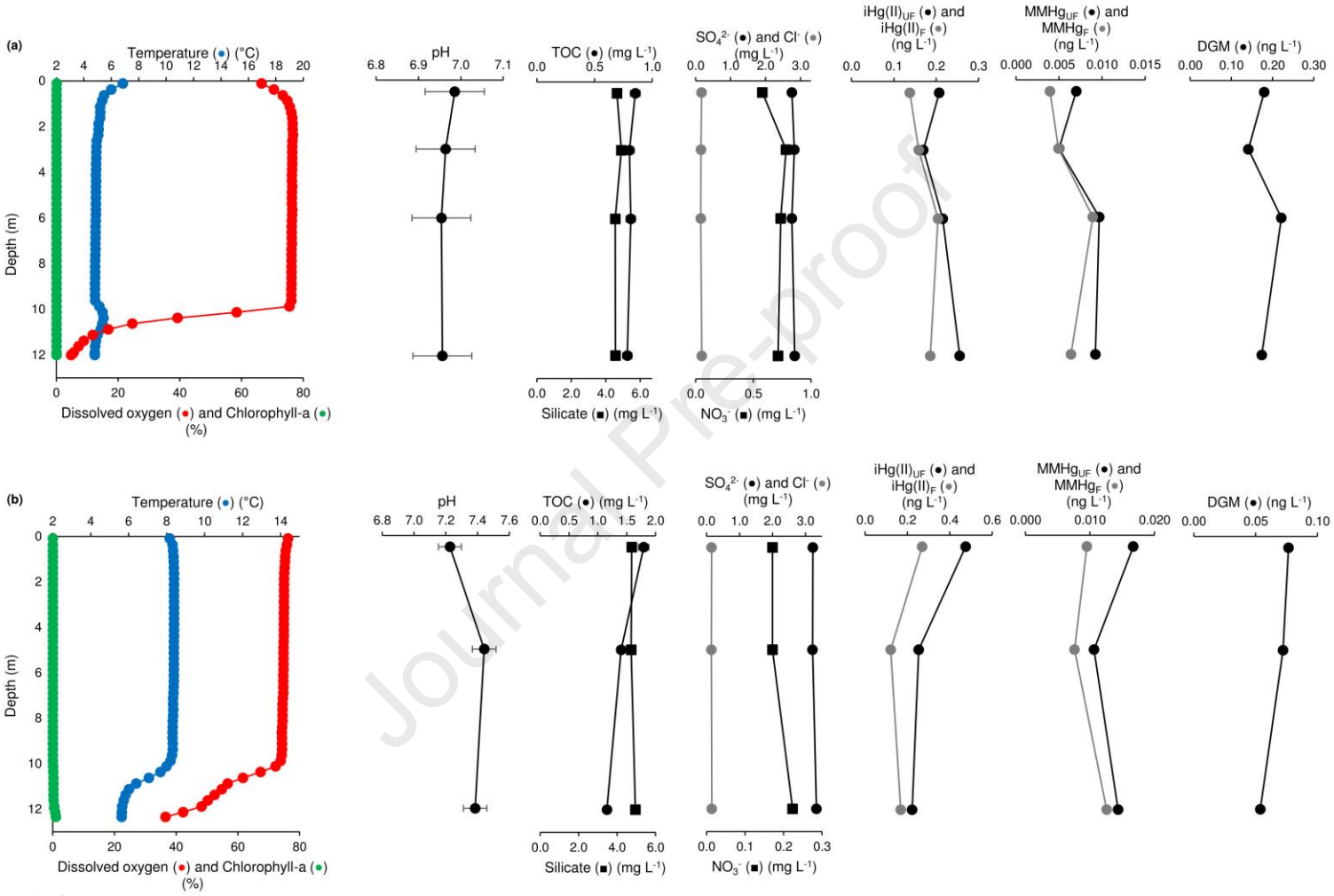

Figure A5: Depth profiles of temperature, percentage of dissolved oxygen saturation, chlorophyll-a (RFU) and some other chemical parameters including mercury speciation obtained in (a) June 2018 and (b) October 2018 in Lake Arratille.

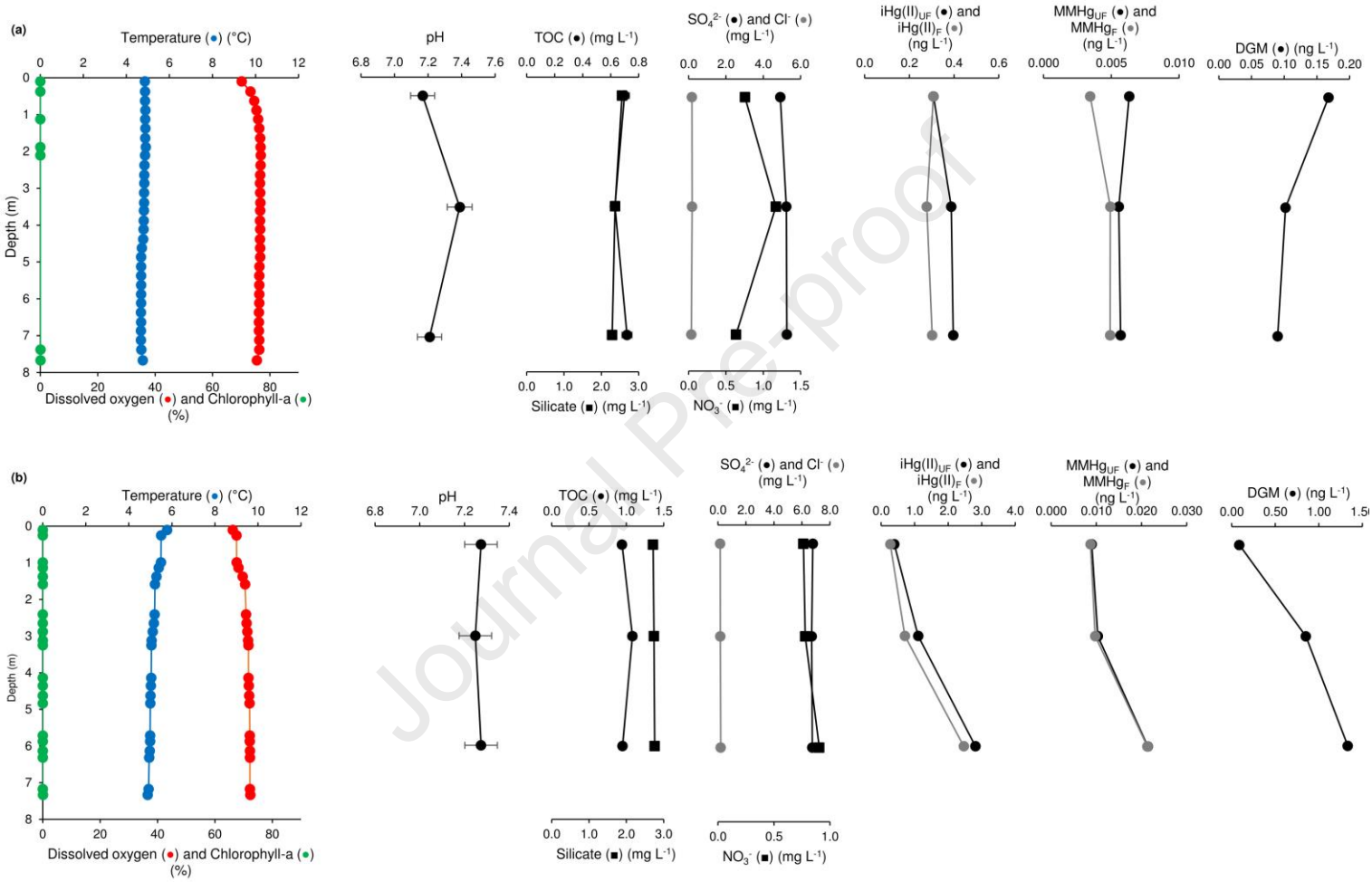

Figure A6: Depth profiles of temperature, percentage of dissolved oxygen saturation, chlorophyll-a (RFU) and some other chemical parameters including mercury speciation obtained in (a) June 2018 and (b) October 2018 in Lake Azul.

251

252

253

254

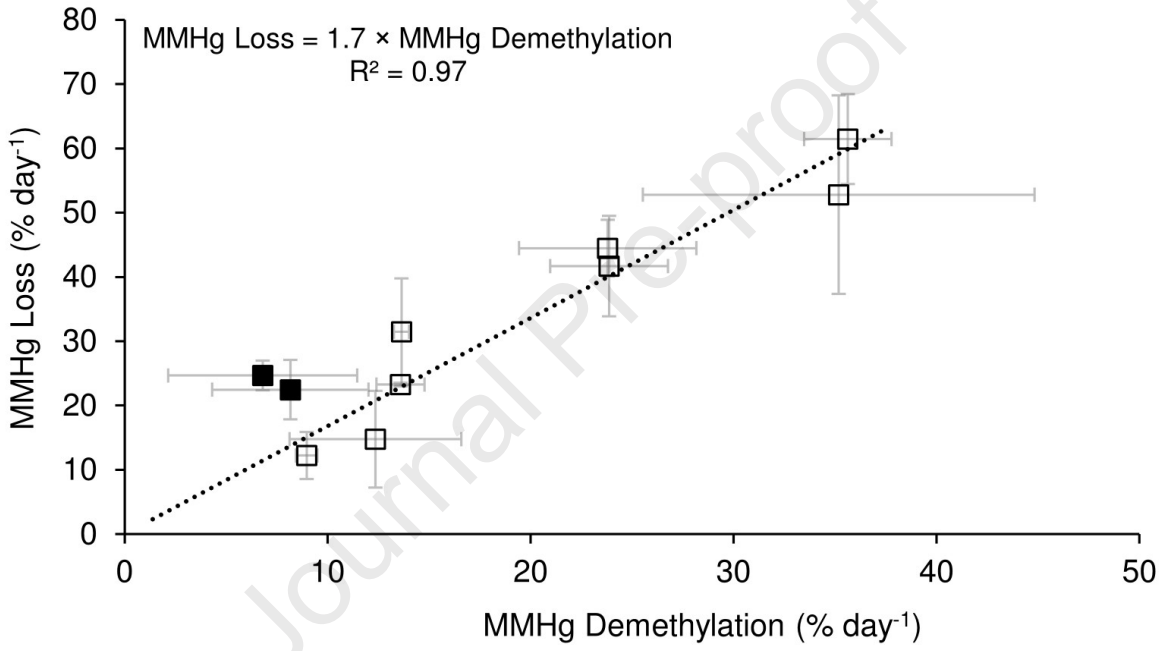

Figure A7: Linear relationship between MMHg Demethylation and MMHg Loss. The two black squares, out of the trend, correspond to MMHg demethylation / MMHg loss under dark conditions in the middle depth of Lake Sabocos (June 2019).

Table A1: Some physical characteristics of the sampled lakes. Note that max depth was either measured or estimated from size using allometric relation, and volume of the lakes was also estimated from max depth using a geometric approximation (error can be large). Pre-Devonian Granitic rocks (pDe-GR), Devonian sedimentary rocks (De-SR) include limestone, sandstone and shale. Permo-Triassic sedimentary rocks (PT-SR) include conglomerate, sandstone, lutite, and andesite. Cretaceous sedimentary rocks (Cr-SR) are mainly composed by carbonate rocks.

Lake name	ID Lake	Latitude	Longitude	Elevation (m asl)	Size (Ha)	Catchment (Ha)	Max depth (m) (*calculated)	Volume (m^3) (calculated)	Prevailing bedrock
Cauterets area									
Lac d'Arratille	**ARA**	42.8009	-0.1748	2256	5.87	296.4	12	264307	De-SR
Lac de la Badète	**BAD**	42.7938	-0.1820	2341	6.97	79.9	7	243990	De-SR
Grand lac de Cambalès	**CAM**	42.8297	-0.2251	2344	3.46	179.7	15	208745	pDe-GR
Lac de Peyregnets de Cambalès	**PEY**	42.8324	-0.2379	2493	1.17	15.2	9	52987	pDe-GR
Lac de Petite Opale	**OPA**	42.8284	-0.2177	2290	0.64	129.3	6*	25788	pDe-GR
Lac Nère	**NER**	42.8350	-0.2029	2304	2.91	94.8	12	178522	pDe-GR
Lac de Pourtet	**POU**	42.8432	-0.2031	2403	5.95	48.7	13	387705	pDe-GR
Ayous Area									
Lac Gentau	**GEN**	42.8482	-0.4874	1942	8.62	186.2	20	993736	PT-SR
Lac Roumassot	**ROU**	42.8480	-0.4793	1843	5.15	268.2	16	424200	PT-SR
Lac Bersau	**BER**	42.8392	-0.4952	2080	12.82	61.4	35	2266475	PT-SR

Table A1 (continued)

Panticosa Area									
Ibón de Arnales	**ARN**	42.7738	-0.2435	2320	2.60	93.5	9	84579	pDe-GR
Ibón de Ordicuso Inferior	**ORD**	42.7571	-0.2478	2100	0.37	14.9	3	14171	De-SR
Ibón de los Baños de Panticosa	**PAN**	42.7589	-0.2370	1640	5.50	3229	15	470072	pDe-GR
Ibón Azul Alto	**AZU**	42.7898	-0.2461	2420	3.89	151.4	8	273527	De-SR
Ibón de Pecico de la Canal	**PEC**	42.7992	-0.2251	2460	0.91	167.5	9*	38954	De-SR
Ibón de Xuans	**XUA**	42.7773	-0.2090	2600	2.97	41.3	15	183875	pDe-GR
Ibón de Coanga	**COA**	42.7774	-0.2199	2304	0.58	27.9	5	23208	pDe-GR
Ibón de Bachimaña Bajo	**BAC**	42.7813	-0.2266	2178	3.08	1470.1	13*	193335	pDe-GR
Ibón de Sabocos	**SAB**	42.6926	-0.2574	1900	9.56	231.7	25	1183798	Cr-SR

Table A2: Main chemical parameters of the studied lakes measured by the multiparametric probe (temperature, conductivity, redox potential), the TOC analyser (TOC as NPOC), the VINDTA 3C Instrument (DIC) and the ionic chromatograph (Cl^-, NO_3^-, and SO_4^{2-}). pH was calculated according to *Kortazar et al.*[4]. Associated error corresponds to standard deviation of three replicated (n=3) points sampled per lake (June 2017 and October 2017).

Lake	Cl^-	NO_3^-	SO_4^{2-}	T	Cond.	pH	E	NPOC	DIC
	mg L^{-1}			° C	µS cm^{-1}		mV	mg C L^{-1}	µmol kg^{-1}
Cauterets Area – June 2017									
ARA	0.20 ± 0.03*	0.64 ± 0.03*	2.90 ± 0.03*	9.53	46	7.35 ± 0.02*	271	1.57 ± 0.19*	680 ± 3*
BAD	0.20 ± 0.04*	0.77 ± 0.01*	3.59 ± 0.06*	n.d.	n.d.	7.46	n.d.	2.00 ± 0.17*	787 ± 3*
CAM	0.17 ± 0.01*	0.40 ± 0.06*	0.39 ± 0.01*	8.71	8	6.42 ± 0.02*	160	0.68 ± 0.05*	124 ± 2*
PEY	0.16 ± 0.01*	0.41 ± 0.06*	0.28 ± 0.03*	5.45	17	6.01 ± 0.01*	208	0.63 ± 0.01*	92 ± 3*
OPA	0.16	0.65 ± 0.08*	0.51 ± 0.01*	n.d.	n.d.	6.92 ± 0.01*	n.d.	1.06 ± 0.07*	308 ± 4*
NER	0.16 ± 0.01*	0.30 ± 0.08*	0.38 ± 0.01*	11.13	7	6.27 ± 0.04*	119	0.78 ± 0.01*	109 ± 2*
POU	0.23 ± 0.03*	0.40 ± 0.03*	0.43 ± 0.01*	9.46	12	6.75 ± 0.05*	202	1.02 ± 0.17*	190 ± 1*
Cauterets Area – October 2017									
ARA	0.15 ± 0.01*	0.21 ± 0.02*	3.74 ± 0.04*	9.85	65	7.91 ± 0.03*	80	2.80 ± 0.35*	822 ± 3*
BAD	0.20 ± 0.05*	0.41 ± 0.08*	3.72 ± 0.11*	9.72	67	7.59 ± 0.04*	46	3.05 ± 0.59*	858 ± 14*
CAM	0.19 ± 0.01*	0.21 ± 0.01*	0.63 ± 0.02*	9.71	14	6.65 ± 0.03*	121	1.27 ± 0.22*	172 ± 2*
PEY	0.17 ± 0.01*	<LoD*	0.35 ± 0.03*	9.57	7	6.00	108	1.40	87
OPA	0.16 ± 0.01*	0.58 ± 0.04*	0.71 ± 0.02*	9.89	25	6.93 ± 0.04*	141	1.32 ± 0.06*	322 ± 3*
Cauterets Area – June 2018									
ARA-t1	0.27	0.85	2.64	5.86	38	7.09	176	0.88	597
ARA-t2	0.17	0.58	2.75	5.70	38	6.99	84	0.85	597
ARA-t3	0.18	0.71	2.65	5.72	35	6.94	317	0.79	590
ARA-t4	0.19	0.61	2.80	6.64	36	6.88	310	0.82	580
BAD	0.19	1.13	5.43	5.89	34	7.21	207	0.89	915
CAM	0.13	0.34	0.35	2.43	5	5.80	172	0.85	108
CAM-meltwater	n.d.	n.d.	n.d.	n.d.	n.d.	n.d.	n.d.	1.03	315
CAM-ice	n.d.	n.d.	n.d.	n.d.	n.d.	n.d.	n.d.	3.34	52
PEY	0.07	0.10	<LoD	6.41	16	4.87	36	0.84	33
OPA	0.17	0.56	0.49	3.29	15	6.48	91	0.71	270

Table A2 (continued)

Cauterets Area – October 2018									
ARA	0.15	0.17	3.23	8.32	50	7.23	170	1.79	777
BAD	0.15	0.29	2.96	5.33	45	7.37	136	1.26	778
CAM	0.18	0.21	0.40	8.47	10	6.36	222	1.08	162
PEY	0.14	<LoD	<LoD	6.81	5	5.94	151	1.64	79
OPA	0.17	0.51	0.48	5.90	17	6.74	127	1.13	307
Ayous Area – June 2018									
GEN-t1	0.25	0.10	0.49	6.89	20	6.70	269	0.85	341
GEN-t2	0.36	0.18	0.42	6.87	20	6.72	202	0.86	346
GEN-t3	0.26	0.21	0.49	6.87	20	6.90	202	0.62	339
GEN-t4	0.38	0.16	0.47	7.21	20	6.64	75	1.09	340
ROU	0.30	0.14	0.50	n.d.	n.d.	n.d.	n.d.	0.87	345
BER	0.23	0.37	0.32	n.d.	n.d.	n.d.	n.d.	0.77	168
Ayous Area – October 2018									
GEN-t1	0.30	<LoD	<LoD	12.63	24	6.74	166	1.30	368
GEN-t2	0.26	<LoD	0.31	12.80	24	6.75	96	1.38	358
GEN-t3	0.37	<LoD	0.38	12.81	24	6.71	137	1.25	359
ROU	0.29	<LoD	0.47	13.38	25	6.85	36	1.86	359
BER	0.31	<LoD	<LoD	12.09	15	7.43	38	1.58	237
Ayous Area – June 2019									
GEN-t1	0.27	0.33	0.55	7.17	30	n.d.	234	1.50	n.d.
GEN-t2	0.32	0.44	0.59	7.57	30	n.d.	285	1.15	n.d.
GEN-t3	0.29	0.29	0.49	7.57	30	n.d.	285	1.16	n.d.
GEN-t4	0.27	0.33	0.51	8.53	32	n.d.	240	1.15	n.d.
ROU	0.26	0.30	0.58	12.69	34	n.d.	234	1.45	n.d.
BER	0.24	0.22	<LoD	2.14	9	n.d.	206	1.12	n.d.

Table A2 (continued)

Panticosa Area – June 2017									
ARN	0.17 ± 0.01*	0.66 ± 0.01*	1.40 ± 0.02*	8.43	18	6.83 ± 0.02*	122	1.03 ± 0.13*	225 ± 1*
ORD	0.18 ± 0.01*	0.12 ± 0.03*	1.86 ± 0.09*	18.29	61	7.34 ± 0.03*	157	2.74 ± 0.39*	695 ± 32*
PAN	0.33 ± 0.09*	0.73 ± 0.13*	2.29 ± 0.14*	10.29	27	7.02	195	1.54 ± 0.17*	402
AZU	0.20 ± 0.02*	0.89 ± 0.16*	6.51 ± 0.04*	8.22	58	7.47	131	2.14 ± 0.22*	797
PEC	0.18 ± 0.01*	0.79 ± 0.06*	2.61 ± 0.04*	8.84	36	7.13 ± 0.02*	198	1.51 ± 0.02*	457 ± 2*
XUA	0.20 ± 0.04*	0.90 ± 0.06*	0.61 ± 0.03*	4.63	12	6.68 ± 0.02*	110	0.85 ± 0.05*	202 ± 5*
COA	0.15 ± 0.01*	0.21 ± 0.02*	0.47 ± 0.02*	7.11	23	6.42	97	1.02 ± 0.05*	134
BAC	0.23 ± 0.01*	0.69 ± 0.15*	1.71 ± 0.04*	-	-	6.94 ± 0.02*	-	1.23 ± 0.09*	310 ± 3*
Panticosa Area – October 2017									
ARN	0.19 ± 0.01*	0.66 ± 0.02*	2.72 ± 0.07*	10.19	31	7.07 ± 0.03*	117	1.61 ± 0.35*	356 ± 3*
PAN	0.33 ± 0.11*	0.43 ± 0.01*	2.57 ± 0.25*	11.12	51	7.02 ± 0.07*	146	2.06 ± 0.26*	430 ± 5*
AZU	0.17 ± 0.01*	0.68 ± 0.03*	7.56 ± 0.05*	8.77	72	7.60 ± 0.05*	102	2.50 ± 0.10*	882 ± 6*
COA	0.20 ± 0.01*	<LoD*	0.57 ± 0.03*	11.08	15	6.67 ± 0.05*	81	1.90 ± 0.11*	190 ± 5*
BAC	0.18 ± 0.01*	0.37 ± 0.02*	2.35 ± 0.05*	10.71	36	7.10 ± 0.05*	114	1.80 ± 0.28*	413 ± 12*
Panticosa Area – June 2018									
ARN	0.19	0.62	1.13	7.45	13	6.33	200	0.77	184
ORD	0.20	0.20	1.86	17.50	57	7.02	97	2.26	722
PAN	0.27	0.71	1.88	11.18	28	6.67	176	1.01	359
AZU-t1	0.18	0.76	4.91	4.87	46	7.17	149	0.70	675
AZU-t2	0.17	0.69	4.76	5.03	43	n.d.	39	0.65	661
PEC	0.17	1.03	1.68	4.33	21	6.64	149	0.65	314
COA	0.24	0.41	0.35	10.09	7	5.85	169	1.03	108
BAC	0.16	0.57	1.68	12.45	25	6.55	129	0.94	290
SAB	0.21	0.49	2.33	17.25	115	7.53	207	1.71	1723

Table A2 (continued)

Panticosa Area – October 2018									
ARN	0.21	0.81	2.19	7.41	20	6.79	221	-	309
ORD	0.39	0.14	1.50	9.32	48	6.90	225	4.63	573
PAN	0.68	0.63	2.20	9.87	25	6.64	193	2.03	372
AZU	0.16	0.76	6.78	5.39	50	7.27	110	0.94	803
PEC	0.19	0.69	2.39	8.13	35	6.79	216	1.08	444
COA	0.25	0.09	<LoD	6.18	7	6.02	163	1.87	125
BAC	0.22	0.82	1.89	8.97	32	6.75	207	1.05	358
SAB-t1	0.23	0.13	2.48	10.42	100	7.71	188	3.02	1691
SAB-t2	0.20	0.37	2.54	10.70	101	7.64	245	1.96	1694
SAB-t3	0.22	<LoD	2.56	10.80	101	7.67	262	2.62	1692
Panticosa Area – June 2019									
SAB-t1	0.15	0.73	2.62	12.47	141	n.d.	212	1.86	n.d.
SAB-t2	0.15	0.66	2.49	11.87	130	n.d.	138	1.79	n.d.
SAB-t3	0.15	0.76	2.55	11.87	130	n.d.	138	1.80	n.d.

Table A3: Filtered and unfiltered inorganic mercury (iHg(II)), monomethylmercury (MMHg) and Dissolved Gaseous Mercury (DGM) concentrations measured in the subsurface water samples of the 19 studied lakes. Volatilization flux densities (*FD*) are calculated according to the methodology detailed in *Sharif et al.* [5] for DGM fluxes and using the specific gas exchange model for sheltered lakes developed by *Cole and Caraco* [6]. Associated error corresponds to standard deviation of three replicated (n=3) points sampled per lake (June 2017 and October 2017). ^{Ø} correspond to outlier (Grubbs's test).

Lake	$iHg(II)_F$	$iHg(II)_{UF}$	$MMHg_F$	$MMHg_{UF}$	DGM	FD (1m s^{-1})	FD (3m s^{-1})
			ng L^{-1}			ng m^{-2} day^{-1}	ng m^{-2} day^{-1}
Cauterets Area – June 2017							
ARA	0.15	0.26 ± 0.01*	0.011 ± 0.001*	0.012 ± 0.001*	0.33	178	270
BAD	0.16 ± 0.03*	0.27 ± 0.03*	<LoD	0.009 ± 0.001*	0.02	7	11
CAM	0.26 ± 0.02*	0.38 ± 0.03*	<LoD	0.018 ± 0.002*	0.12	61	93
PEY	0.19 ± 0.02*	0.31 ± 0.09*	0.012	0.014 ± 0.003*	0.12	60	92
OPA	0.11 ± 0.01*	0.12 ± 0.01*	0.007	0.007 ± 0.002*	0.07	34	52
NER	0.41 ± 0.05*	0.47 ± 0.02*	0.008	0.010 ± 0.002*	0.13	68	103
POU	0.26 ± 0.03*	0.44 ± 0.07*	<LoD	0.010 ± 0.002*	0.11	57	86
Cauterets Area – October 2017							
ARA	0.12 ± 0.02*	0.15 ± 0.02*	0.005 ± 0.001*	0.006 ± 0.001*	0.04	20	30
BAD	0.34 ± 0.27*	0.46 ± 0.12*	0.004 ± 0.001*	0.006 ± 0.001*	0.26	141	214
CAM	0.50 ± 0.05*	0.51 ± 0.06*	0.006 ± 0.002*	0.009 ± 0.002*	0.42	233	352
PEY	0.17 ± 0.05*	0.29 ± 0.02*	<LoD	0.006 ± 0.002*	0.12	65	98
OPA	0.22 ± 0.03*	0.42 ± 0.11*	0.004 ± 0.001*	0.006 ± 0.001*	0.10	50	75
Cauterets Area – June 2018							
ARA-t1	0.08	0.11	0.005	0.007	0.05	24	37
ARA-t2	0.14	0.21	0.004	0.007	0.18	96	146
ARA-t3	0.17	0.17	0.007	0.007	0.20	106	160
ARA-t4	0.15	0.20	0.004	0.010	0.12	60	91
BAD	0.16	0.18	0.005	0.006	0.12	62	95
CAM	0.19	0.26	0.009	0.012	0.19	100	152
CAM-meltwater	0.53	1.01	0.010	0.035	n.d.	n.d.	n.d.
CAM-ice	1.03	18.80	0.054	0.612	n.d.	n.d.	n.d.
PEY	0.31	0.67	0.015	0.023	0.39	217	328
OPA	0.19	0.24	0.007	0.007	0.04	19	29

Table A3 (continued)

Cauterets Area – October 2018							
ARA	0.27	0.47	0.010	0.017	0.08	38	58
BAD	0.23	0.28	0.010	0.010	0.04	19	29
CAM	0.19	0.45	0.008	0.011	0.09	44	67
PEY	0.20	0.40	0.009	0.010	0.09	48	72
OPA	0.20	0.31	0.008	0.009	0.06	27	41
Ayous Area – June 2018							
GEN-t1	0.16	0.84	0.007	0.008	0.09	46	69
GEN-t2	0.21	0.38	0.006	0.008	10.79[ø]	6090	9226
GEN-t3	0.19	0.68	0.009	0.013	0.26	143	216
GEN-t4	0.17	0.39	0.009	0.014	0.26	140	213
ROU	0.18	0.30	0.014	0.014	0.13	n.d.	n.d.
BER	0.35	0.70	0.016	0.018	0.27	n.d.	n.d.
Ayous Area – October 2018							
GEN-t1	0.12	0.24	0.024	0.024	0.03	12	18
GEN-t2	0.13	0.31	0.026	0.029	0.06	30	46
GEN-t3	0.14	0.16	0.026	0.027	0.04	19	29
ROU	0.21	0.38	0.017	0.034	0.03	14	22
BER	0.17	0.21	0.005	0.007	0.05	21	32
Ayous Area – June 2019							
GEN-t1	0.17	0.24	0.012	0.018	0.09	43	65
GEN-t2	0.18	0.27	0.015	0.012	0.10	50	75
GEN-t3	0.16	0.30	0.014	0.011	0.10	52	79
GEN-t4	0.19	0.25	0.006	0.014	0.10	50	76
ROU	0.29	0.42	0.012	0.025	0.17	90	136
BER	0.41	0.55	0.012	0.021	0.23	126	191

Table A3 (continued)

Panticosa Area – June 2017							
ARN	0.18 ± 0.02*	0.31 ± 0.02*	<LoD	<LoD	0.06	26	39
ORD	0.52 ± 0.04*	0.73 ± 0.13*	0.014 ± 0.005*	0.047 ± 0.003*	0.18	98	148
PAN	0.24 ± 0.03*	0.34 ± 0.05*	0.006	0.012 ± 0.002*	0.10	54	82
AZU	0.09 ± 0.02*	0.24 ± 0.13*	<LoD	<LoD	0.06	29	44
PEC	0.24 ± 0.01*	0.27 ± 0.03*	<LoD	0.007 ± 0.002*	0.04	17	26
XUA	0.29 ± 0.04*	0.49 ± 0.12*	0.008 ± 0.001*	0.024 ± 0.002*	0.13	70	106
COA	0.43 ± 0.17*	0.60 ± 0.07*	<LoD	0.011 ± 0.001*	0.20	109	165
BAC	n.d.	0.36 ± 0.07*	n.d.	0.008 ± 0.001*	n.d.	n.d.	n.d.
Panticosa Area – October 2017							
ARN	0.23 ± 0.11*	0.36 ± 0.13*	<LoD	0.004 ± 0.001*	0.15	78	119
PAN	0.64 ± 0.15*Ø	1.19 ± 0.17*Ø	0.010 ± 0.003*	0.016 ± 0.002*	0.68Ø	375	568
AZU	0.28 ± 0.01*	0.38 ± 0.06*	<LoD	0.005 ± 0.001*	0.21	111	168
COA	0.53 ± 0.05*	0.72 ± 0.03*	0.006 ± 0.001*	0.012 ± 0.002*	0.37	200	303
BAC	0.23 ± 0.03*	0.35 ± 0.09*	0.009 ± 0.001*	0.013 ± 0.004*	0.05	25	38
Panticosa Area – June 2018							
ARN	0.31	0.38	0.006	0.007	0.08	39	59
ORD	0.54	0.55	0.027	0.030	n.d.	n.d.	n.d.
PAN	0.36	0.53	0.009	0.011	n.d.	n.d.	n.d.
AZU-t1	0.34	0.31	0.003	0.006	0.17	89	135
AZU-t2	0.31	0.38	0.005	0.006	0.09	48	73
PEC	0.20	0.25	0.006	0.007	0.05	23	34
COA	0.42	0.60	0.009	0.011	0.20	108	164
BAC	0.30	0.44	0.010	0.012	0.11	57	87
SAB-t1	0.58	0.70	0.010	0.012	1.27Ø	693	1050
SAB-t2	0.53	0.64	0.008	0.019	4.65Ø	2553	3867
SAB-t3	0.67	0.73	0.010	0.018	1.18Ø	645	977

Table A3 (continued)

Panticosa Area – October 2018							
ARN	0.37	0.52	0.008	0.011	0.20	110	167
ORD	1.10	1.16	0.023	0.025	0.18	97	147
PAN	0.68	0.96	0.035	0.062	n.d.	n.d.	n.d.
AZU	0.27	0.39	0.009	0.009	0.09	45	68
PEC	0.24	0.34	0.005	0.009	n.d.	n.d.	n.d.
COA	2.68[ø]	2.88[ø]	0.022	0.025	0.20	107	162
BAC	0.33	0.38	0.014	0.026	0.11	56	85
SAB-t1	0.39	0.58	0.025	0.027	0.52	288	436
SAB-t2	0.39	0.58	0.018	0.029	0.29	156	237
SAB-t3	0.44	0.53	0.022	0.029	n.d.	n.d.	n.d.
Panticosa Area – June 2019							
SAB-t1	0.19	0.34	0.005	0.005	0.06	31	46
SAB-t2	0.21	0.32	0.014	0.022	1.34[ø]	741	1122
SAB-t3	0.18	0.35	0.005	0.018	0.16	87	132

Table A4: Filtered and unfiltered inorganic mercury (iHg(II)), monomethylmercury (MMHg) and Dissolved Gaseous Mercury (DGM) concentrations measured in the depth water samples of the 4 intensively studied lakes (Gentau, Sabocos, Arratille and Azul Superior) together with some physicochemical parameters.

Depth	$iHg(II)_F$	$iHg(II)_{UF}$	$MMHg_F$	$MMHg_{UF}$	DGM	Cl^-	NO_3^-	SO_4^{2-}	T	DO	pH	NPOC
m			ng L^{-1}				mg L^{-1}		(°C)	%		mg C L^{-1}
Lake Gentau – June 2018												
0.5	0.21	0.38	0.006	0.008	10.79	0.36	0.18	0.42	6.87	82	6.72	0.86
5	0.20	0.31	0.009	0.010	3.04	0.27	0.18	0.43	4.97	78	6.68	0.75
8	0.18	0.34	0.009	0.013	0.31	0.34	0.04	0.49	4.37	27	6.74	1.03
12	0.18	0.19	0.023	0.057	0.23	0.60	0.03	0.68	4.23	3	6.76	1.41
18	0.66	0.75	0.318	0.426	0.14	0.92	0.08	0.66	4.40	1	6.77	1.44
Lake Gentau – October 2018												
0.5	0.13	0.31	0.026	0.029	0.06	0.26	<LoD	0.31	12.80	79	6.75	1.38
5	0.14	0.15	0.017	0.055	0.06	0.22	<LoD	0.30	12.68	78	6.65	1.34
8	0.14	0.23	0.020	0.041	0.05	0.24	<LoD	0.33	12.62	77	6.77	1.43
12	0.08	0.09	0.011	0.027	0.04	0.55	<LoD	0.47	8.52	33	6.96	2.39
17	0.36	0.39	0.341	0.388	0.03	0.87	0.14	<LoD	6.05	2	6.90	5.60
Lake Gentau – June 2019												
0.5	0.18	0.27	0.015	0.012	0.10	0.32	0.44	0.59	7.57	79	n.d.	1.15
5	0.15	0.20	0.006	0.007	0.08	0.27	0.27	0.54	6.76	84	n.d.	1.21
8	0.07	0.18	0.004	0.037	0.04	0.31	0.18	0.58	5.82	91	n.d.	1.23
12	0.08	0.14	0.019	0.059	0.02	0.45	0.41	0.71	4.51	20	n.d.	1.28
17.5	0.11	0.18	0.157	0.236	0.01	0.53	0.13	0.70	4.30	4	n.d.	1.18

Table A4 (continued)

Lake Sabocos – June 2018												
0.5	0.53	0.64	0.008	0.019	4.65	0.21	0.49	2.33	17.25	102	6.79	1.71
5	0.47	1.29	0.009	0.013	2.36	0.21	0.48	2.51	10.70	82	6.78	2.07
9	0.35	0.42	0.012	0.017	0.31	0.27	0.45	3.21	7.57	61	6.79	1.93
15	0.33	0.55	0.011	0.017	0.22	0.29	0.54	3.07	6.01	49	6.95	1.54
20	0.29	0.39	0.012	0.026	1.43	0.31	0.50	3.02	5.13	8	6.78	1.55
25	0.32	0.56	0.025	0.060	0.56	0.35	0.46	2.74	4.80	1	6.78	1.32
Lake Sabocos – October 2018												
0.5	0.39	0.58	0.018	0.029	0.29	0.20	0.37	2.54	10.70	78	7.64	1.96
4	0.68	0.90	0.015	0.032	0.38	0.22	0.15	2.54	10.56	78	7.73	2.25
8	0.51	0.54	0.024	0.026	0.43	0.22	0.17	2.55	10.53	77	7.55	2.10
12	0.44	0.53	0.012	0.024	0.52	0.30	0.34	3.09	7.87	62	7.60	2.01
18	0.43	0.61	0.015	0.017	1.15	0.46	0.44	3.10	5.97	35	7.64	2.16
23	0.17	0.79	0.015	0.026	0.41	0.30	0.20	3.03	5.70	5	7.34	2.01
Lake Sabocos – June 2019												
0.5	0.21	0.32	0.014	0.022	1.34	0.15	0.76	2.55	11.87	79	n.d.	1.80
5	0.18	0.34	0.010	0.011	0.12	0.13	0.61	2.40	10.18	82	n.d.	1.73
9	0.03	0.08	0.006	0.018	0.11	0.14	0.71	2.79	7.07	76	n.d.	1.71
13	0.02	0.13	0.004	0.020	0.09	0.16	0.78	2.80	6.09	70	n.d.	1.67
18	0.03	0.13	0.005	0.022	004	0.16	0.79	3.02	5.26	48	n.d.	1.62
25	0.03	0.15	0.021	0.052	0.06	0.17	0.57	2.73	4.87	7	n.d.	1.58

Table A4 (continued)

Lake Arratille – June 2018												
0.5	0.14	0.21	0.004	0.007	0.18	0.17	0.58	2.75	5.70	72	6.99	0.85
3	0.16	0.17	0.005	0.005	0.14	0.15	0.78	2.82	4.91	76	6.96	0.80
6	0.20	0.22	0.009	0.010	0.22	0.15	0.74	2.75	4.87	76	6.95	0.81
12	0.19	0.26	0.006	0.009	0.17	0.18	0.71	2.83	4.79	5	6.96	0.78
Lake Arratille – October 2018												
0.5	0.27	0.47	0.010	0.017	0.08	0.15	0.17	3.23	8.32	76	7.23	1.79
5	0.12	0.25	0.008	0.011	0.07	0.14	0.17	3.22	8.38	75	7.44	1.40
12	0.17	0.22	0.013	0.014	0.05	0.16	0.22	3.33	5.64	45	7.39	1.16
Lake Azul – June 2018												
0.5	0.31	0.31	0.003	0.006	0.17	0.18	0.76	4.91	4.87	74	7.17	0.70
3.5	0.28	0.39	0.005	0.006	0.10	0.19	1.17	5.23	4.82	77	7.39	0.63
7	0.30	0.40	0.005	0.006	0.09	0.15	0.64	5.26	4.67	76	7.21	0.72
Lake Azul – October 2018												
0.5	0.27	0.39	0.009	0.009	0.09	0.16	0.76	6.78	5.39	68	7.27	0.94
3	0.71	1.11	0.010	0.010	0.85	0.17	0.78	6.70	5.08	71	7.25	1.08
6	2.46	2.81	0.021	0.021	1.33	0.20	0.90	6.73	4.98	72	7.27	0.95

Table A5: Operating conditions for the incubation experiments. Note that PFA Teflon bottles (Nalgene) were used to allow in-situ transmission of both UV A and B during incubation (of subsurface waters) [5].

Lake name	Sampling Depth	Light exposure	Water temperature (°C)	Incubation time (h)
Lac Gentau, June 2018 • Good weather • Analytes: iHg(II), MMHg and DGM	Subsurface (0.5m)	Diurnal and Dark	6.87	7.4
	Middle depth (8m)	Diurnal and Dark	4.37	8.5
	Bottom (17m)	Dark	4.40	8.7
Lac Gentau, October 2018 • Cold, Rainy morning, Sunny spell midday, Cloudy afternoon • Analytes: iHg(II), MMHg and DGM	Subsurface (0.5m)	Diurnal and Dark	12.80	7.2
	Middle depth (8m)	Diurnal and Dark	12.62	6.0
	Bottom (17m)	Dark	6.05	7.2
Lac Gentau, June 2019 • Cold, Windy, Sunny spell morning • Analytes: iHg(II), MMHg and DGM	Subsurface (0.5m)	Diurnal and Dark	7.57	8.7
	Middle depth (8m)	Diurnal and Dark	5.82	8.5
	Bottom (17m)	Dark	4.30	8.5
Ibón de Sabocos, June 2018 • Good weather • Analytes: iHg(II), MMHg	Subsurface (0.5m)	Diurnal and Dark	17.25	6.3
	Bottom (27m)	Dark	4.80	6.3
Ibón de Sabocos, October 2018 • Cold, Cloudy afternoon • Analytes: iHg(II), MMHg	Subsurface (0.5m)	Diurnal and Dark	10.70	6.3
	Bottom (23m)	Dark	5.70	6.3
Ibón de Sabocos, June 2019 • Windy, Cloudy • Analytes: iHg(II), MMHg and DGM	Subsurface (0.5m)	Diurnal and Dark	11.87	6.8
	Middle depth (9m)	Diurnal and Dark	7.07	6.8
	Bottom (25m)	Dark	4.87	6.8
Lac d'Arratille, June 2018 • Good weather • Analytes: iHg(II), MMHg and DGM	Subsurface (0.5m)	Diurnal and Dark	5.70	6.0
	Middle depth (6m)	Dark	4.87	5.3
Lac d'Arratille, October 2018 • Rain, Wind, Bad weather • Analytes: iHg(II), MMHg and DGM	Subsurface (0.5m)	Diurnal and Dark	8.32	5.3
	Bottom (12m)	Dark	5.64	6.7

References

(1) Bueno, M.; Duval, B.; Tessier, E.; Romero-Rama, A.; Kortazar, L.; Fernandez, L. A.; De Diego, A.; Amouroux, D. Selenium Distribution and Speciation in Waters of Pristine Alpine Lakes from Central-Western Pyrenees (France-Spain). *Environ. Sci.: Processes Impacts* **2022**, 10.1039.D1EM00430A. https://doi.org/10.1039/D1EM00430A.

(2) Alanoca, L.; Amouroux, D.; Monperrus, M.; Tessier, E.; Goni, M.; Guyoneaud, R.; Acha, D.; Gassie, C.; Audry, S.; Garcia, M. E.; Quintanilla, J.; Point, D. Diurnal Variability and Biogeochemical Reactivity of Mercury Species in an Extreme High-Altitude Lake Ecosystem of the Bolivian Altiplano. *Environmental Science and Pollution Research* **2016**, *23* (7), 6919–6933. https://doi.org/10.1007/s11356-015-5917-1.

(3) Zaharescu, D. G.; Hooda, P. S.; Burghelea, C. I.; Palanca-Soler, A. A Multiscale Framework for Deconstructing the Ecosystem Physical Template of High-Altitudes Lakes. 30.

(4) Kortazar, L.; Duval, B.; Liñero, O.; Olamendi, O.; Angulo, A.; Amouroux, D.; de Diego, A.; Fernandez, L. A. Accurate Determination of the Total Alkalinity and the CO2 System Parameters in High-Altitude Lakes from the Western Pyrenees (France – Spain). *Microchemical Journal* **2020**, *152*, 104345. https://doi.org/10.1016/j.microc.2019.104345.

(5) Sharif, A.; Monperrus, M.; Tessier, E.; Bouchet, S.; Pinaly, H.; Rodriguez-Gonzalez, P.; Maron, P.; Amouroux, D. Fate of Mercury Species in the Coastal Plume of the Adour River Estuary (Bay of Biscay, SW France). *Science of The Total Environment* **2014**, *496*, 701–713. https://doi.org/10.1016/j.scitotenv.2014.06.116.

(6) Cole, J. J.; Caraco, N. F. Atmospheric Exchange of Carbon Dioxide in a Low-Wind Oligotrophic Lake Measured by the Addition of SF_6. *Limnology and Oceanography* **1998**, *43* (4), 647–656. https://doi.org/10.4319/lo.1998.43.4.0647.

Highlights

- Hg speciation and cycling was studied in waters of Pyrenean alpine lakes
- Spatial and seasonal variations of Hg levels and speciation remained low
- Hg species transformation rates were measured by in-situ experiments
- Significant Hg methylation was measured in stratified anoxic waters
- Large photochemical reactions and Hg(0) evasion occurred in surface waters
- Climate change and eutrophication can be important drivers of those pathways

Declaration of interests

☒ The authors declare that they have no known competing financial interests or personal relationships that could have appeared to influence the work reported in this paper.

☐ The authors declare the following financial interests/personal relationships which may be considered as potential competing interests: